Electronic Supplementary Material (ESI) for RSC Advances.

Supplementary Information for:

Synthesis of Arrays Containing Porphyrin, Chlorin, and Perylene-Imide Constituents for Panchromatic Light-Harvesting and Charge Separation

Gongfang Hu, Hyun Suk Kang, Amit K. Mandal, Arpita Roy, Christine Kirmaier,
David F. Bocian, Dewey Holten, and Jonathan S. Lindsey

Table of Contents

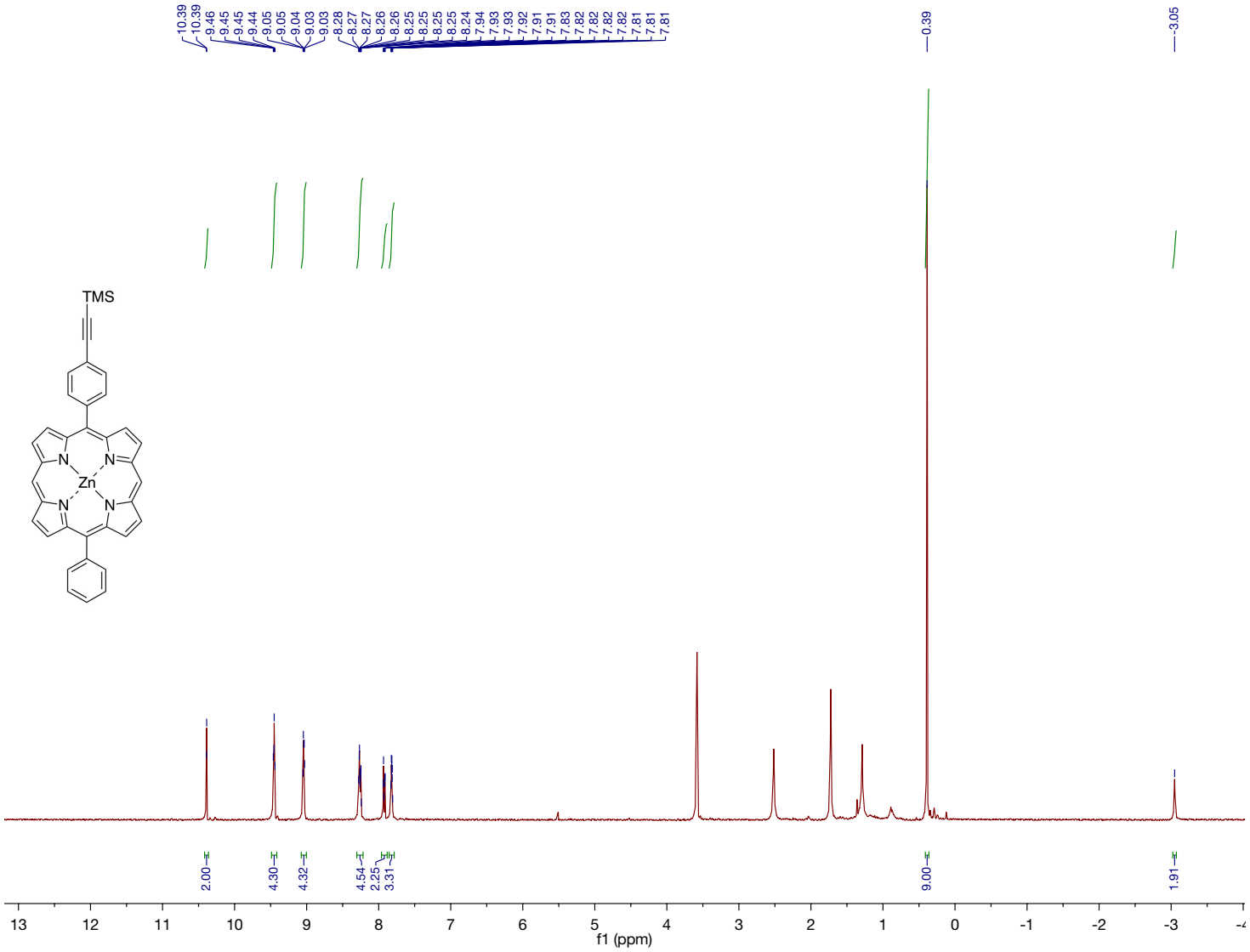

Figure S1. The ^{1}H NMR spectrum of **Zn2-TMS**.

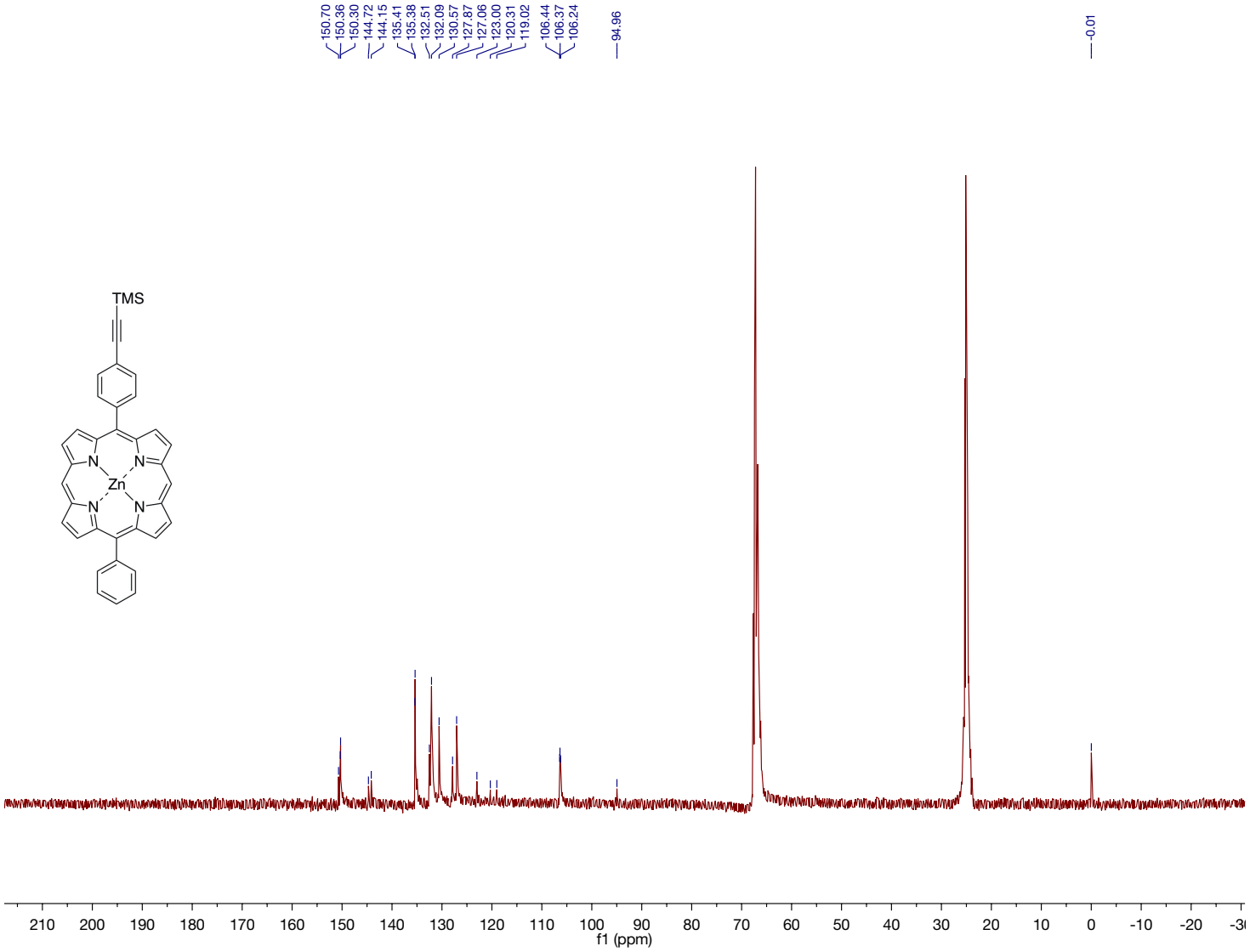

Figure S2. The ^{13}C NMR spectrum of **Zn2-TMS**.

Sample	$M_{Theoretical}$	$M_{Experimental}$	ΔM (ppm)	Elemental Composition
PHGF-II-Zn	621.14475 $[M+H]^+$	621.14281 $[M+H]^+$	-3.113	$C_{37}H_{28}N_4SiZn$

MS Data

PHGF-II-Zn

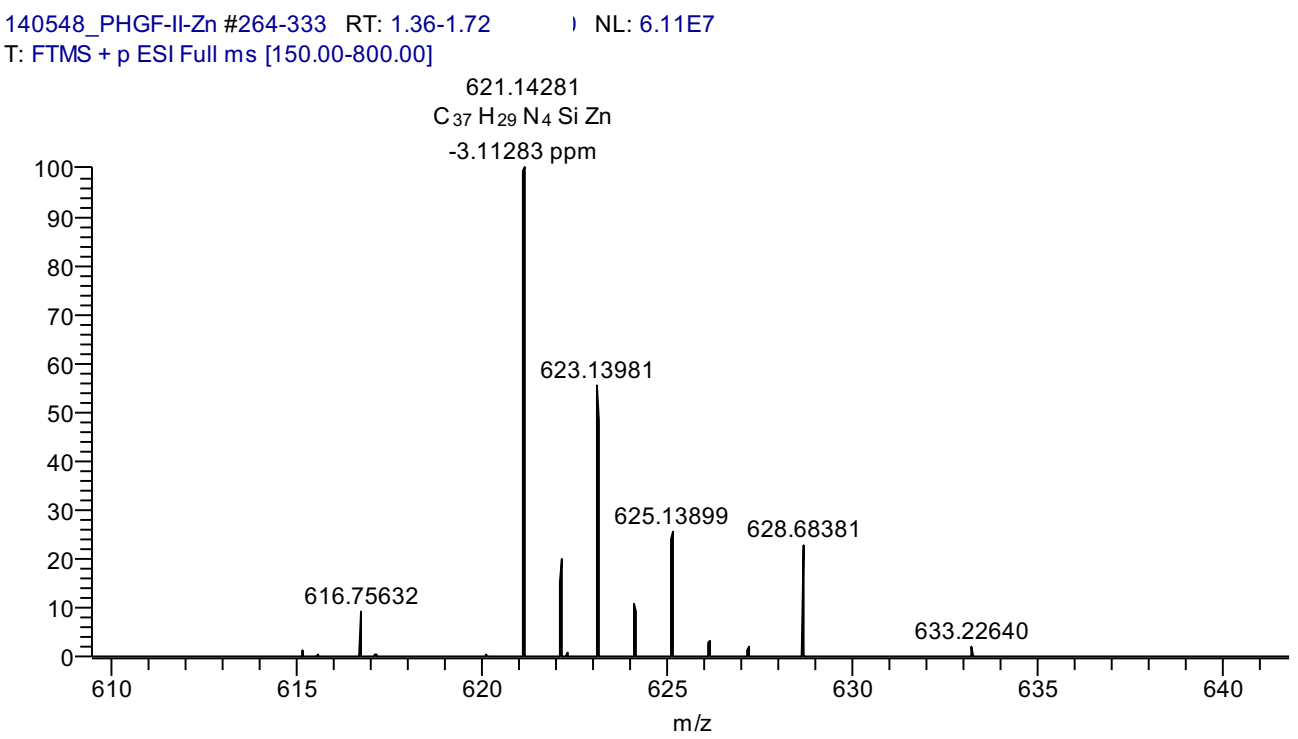

Figure S3. The ESI-MS spectrum of **Zn2-TMS**.

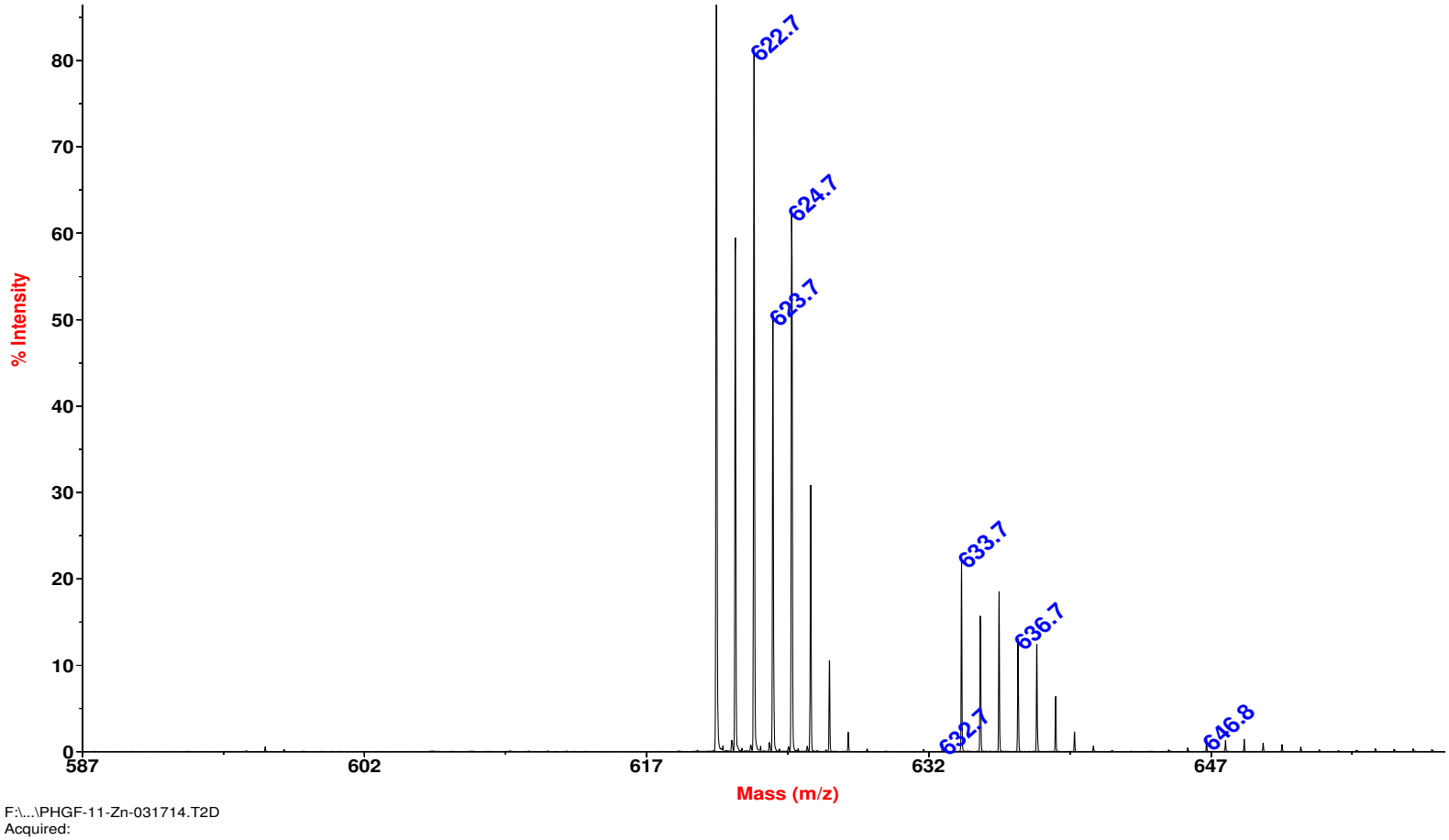

Figure S4. The MALDI-MS spectrum of **Zn2-TMS**.

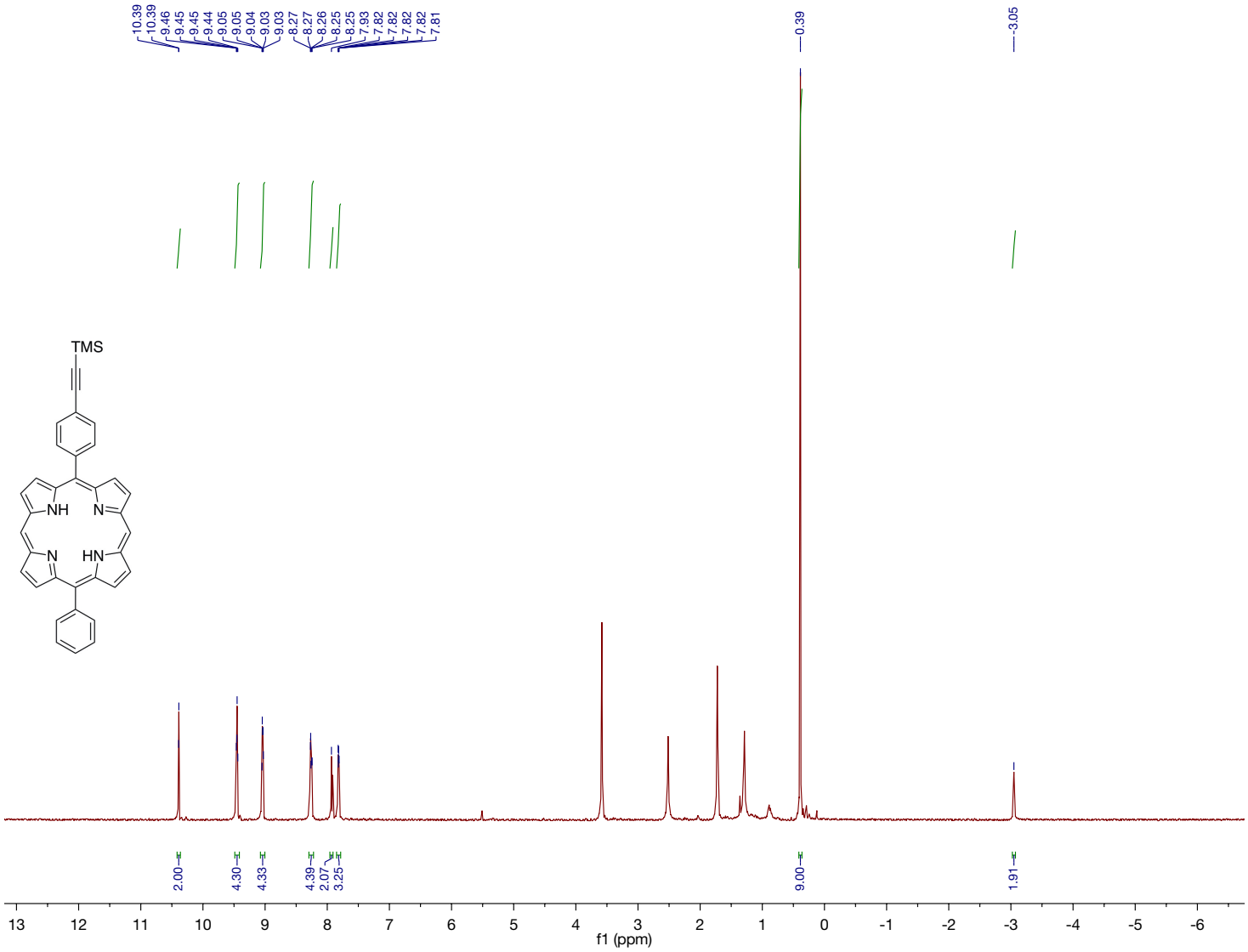

Figure S5. The ^{1}H NMR spectrum of **2-TMS**.

Sample	$M_{Theoretical}$	$M_{Experimental}$	ΔM (ppm)	Elemental Composition
PHGF-II	559.23125 $[M+H]^+$	559.23264 $[M+H]^+$	2.488	$C_{37}H_{30}N_4Si$

MS Data

PHGF-II

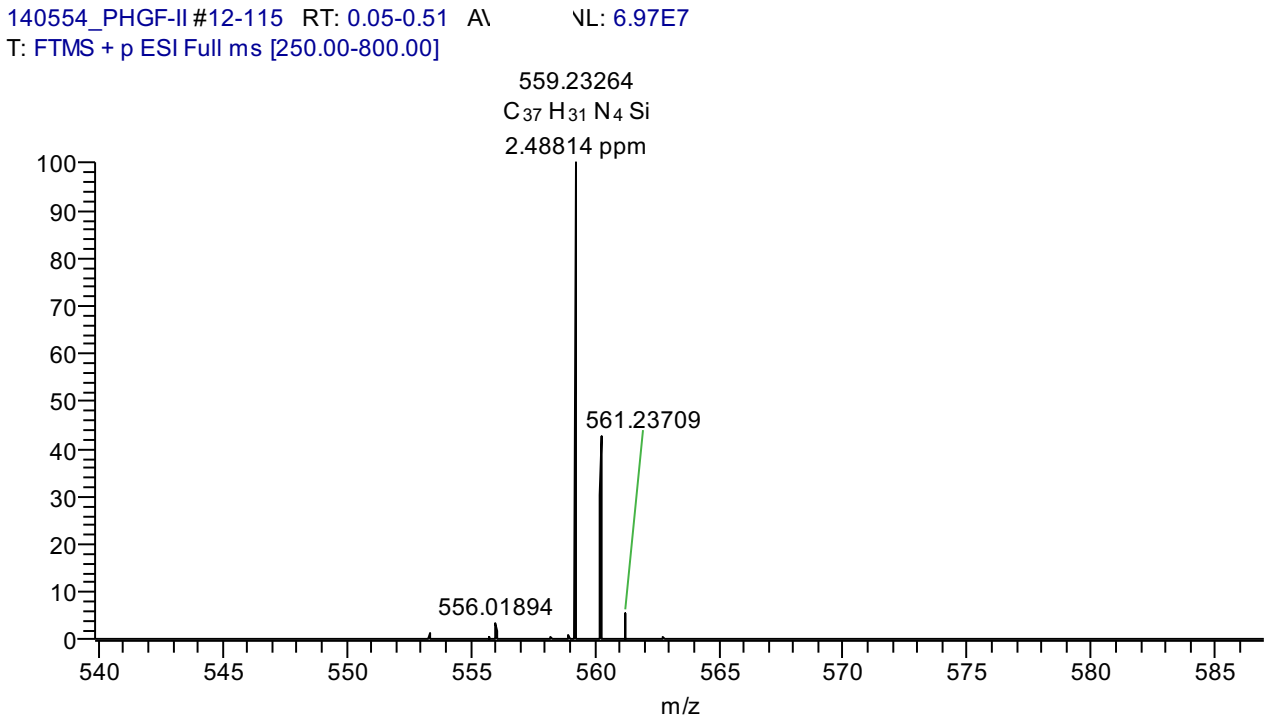

Figure S6. The ESI-MS spectrum of **2-TMS**.

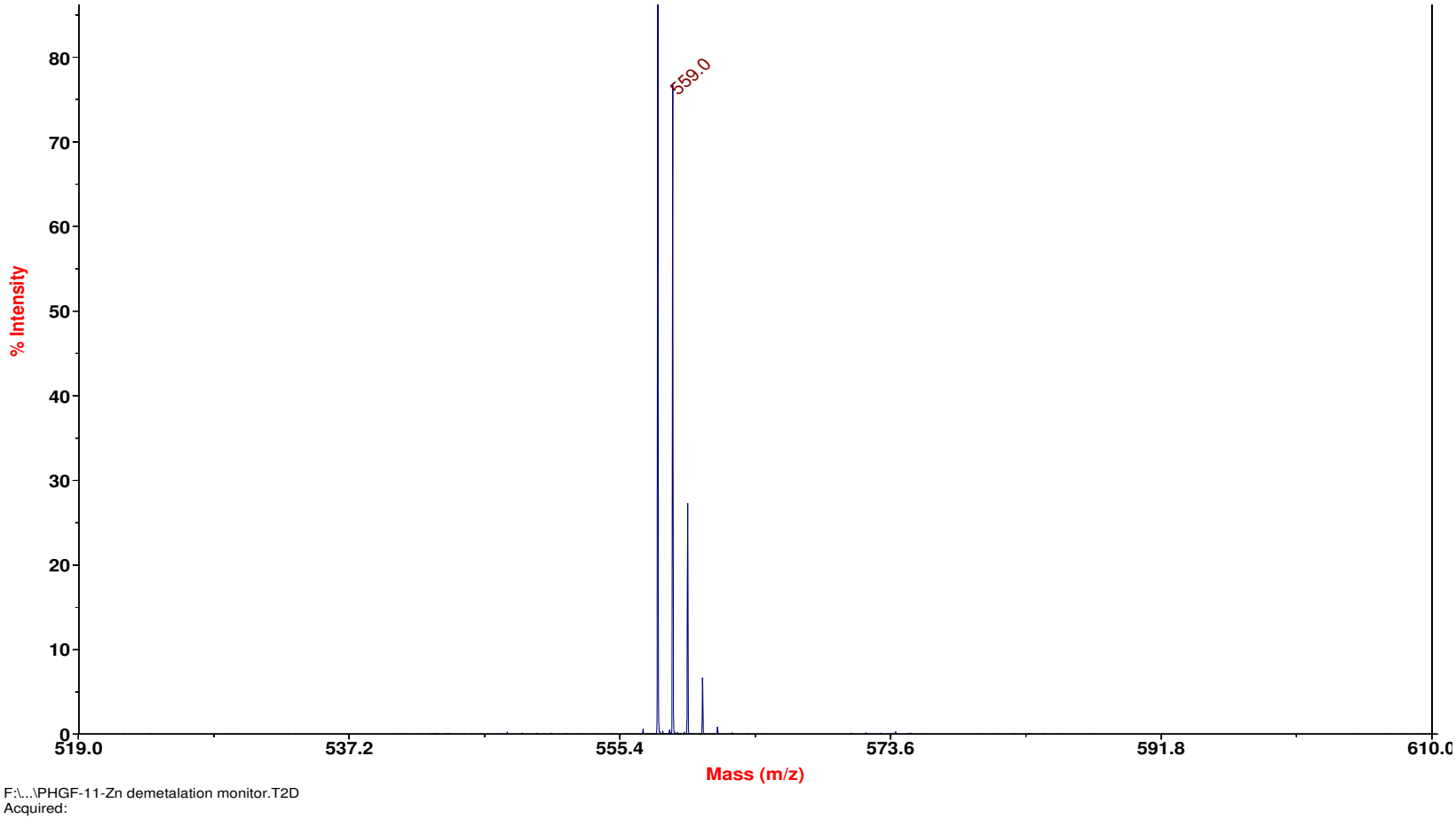

Figure S7. The MALDI-MS spectrum of **2-TMS**.

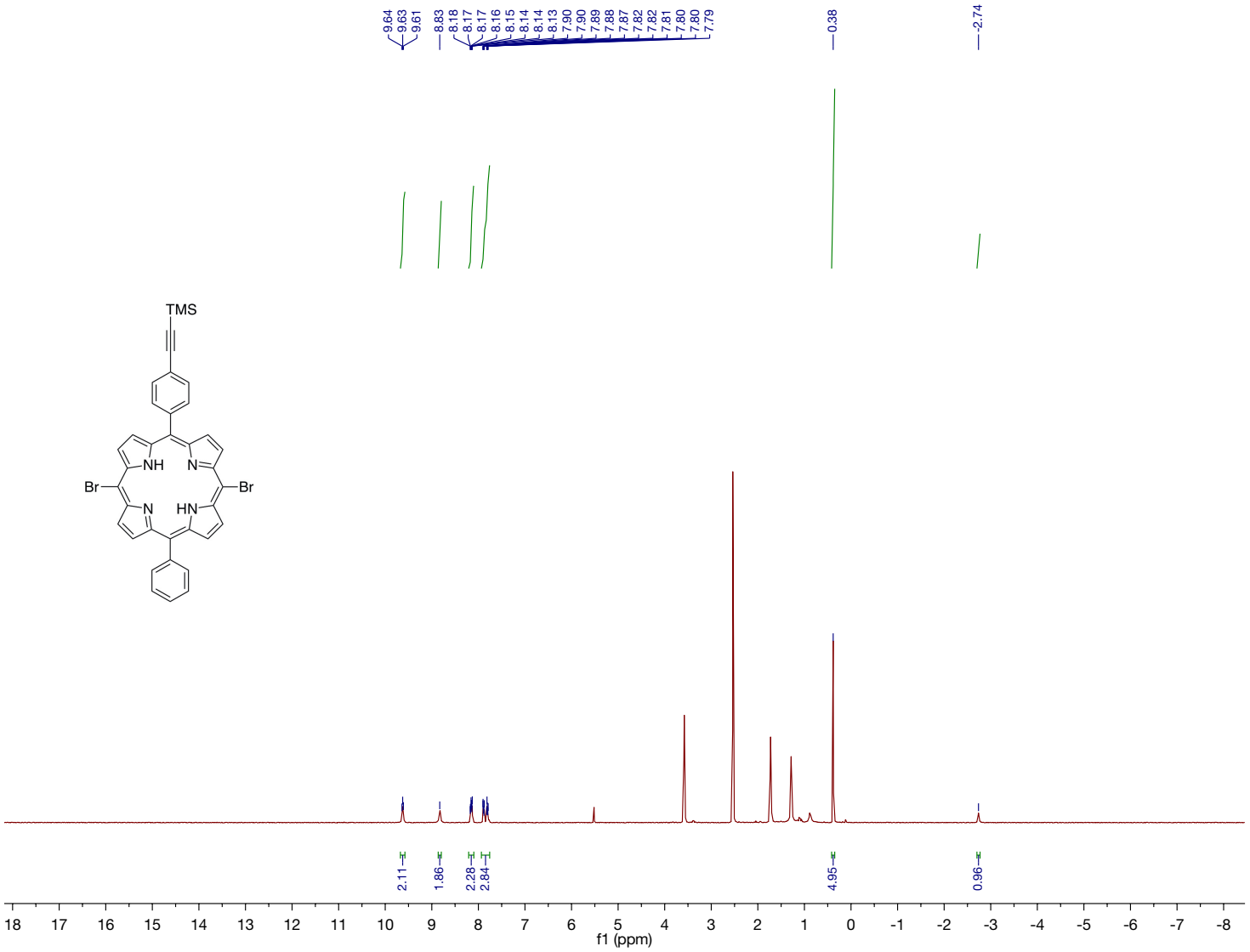

Figure S8. The ^{1}H NMR spectrum of **2-Br$_2$/TMS**.

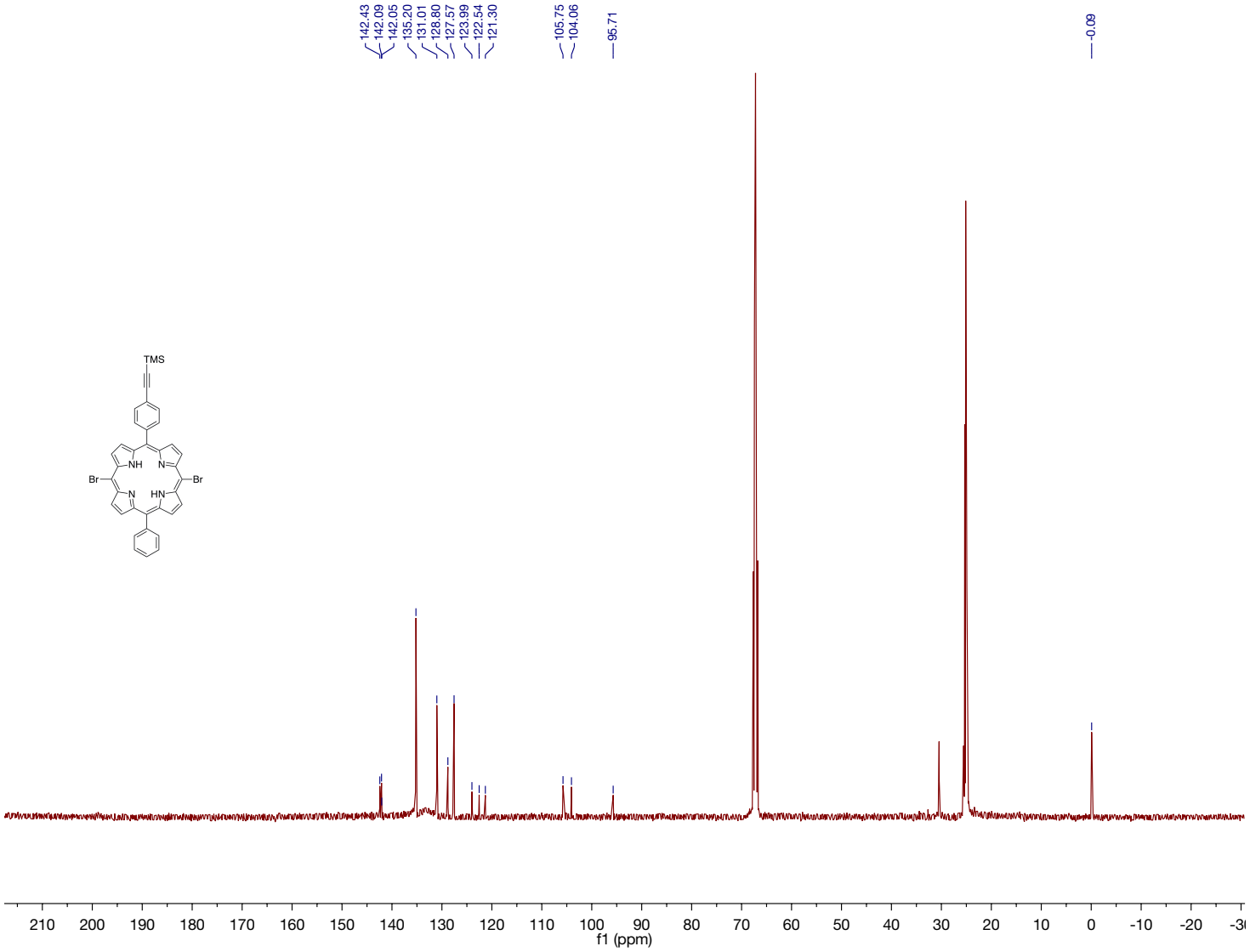

Figure S9. The ^{13}C NMR spectrum of **2-Br$_2$/TMS**.

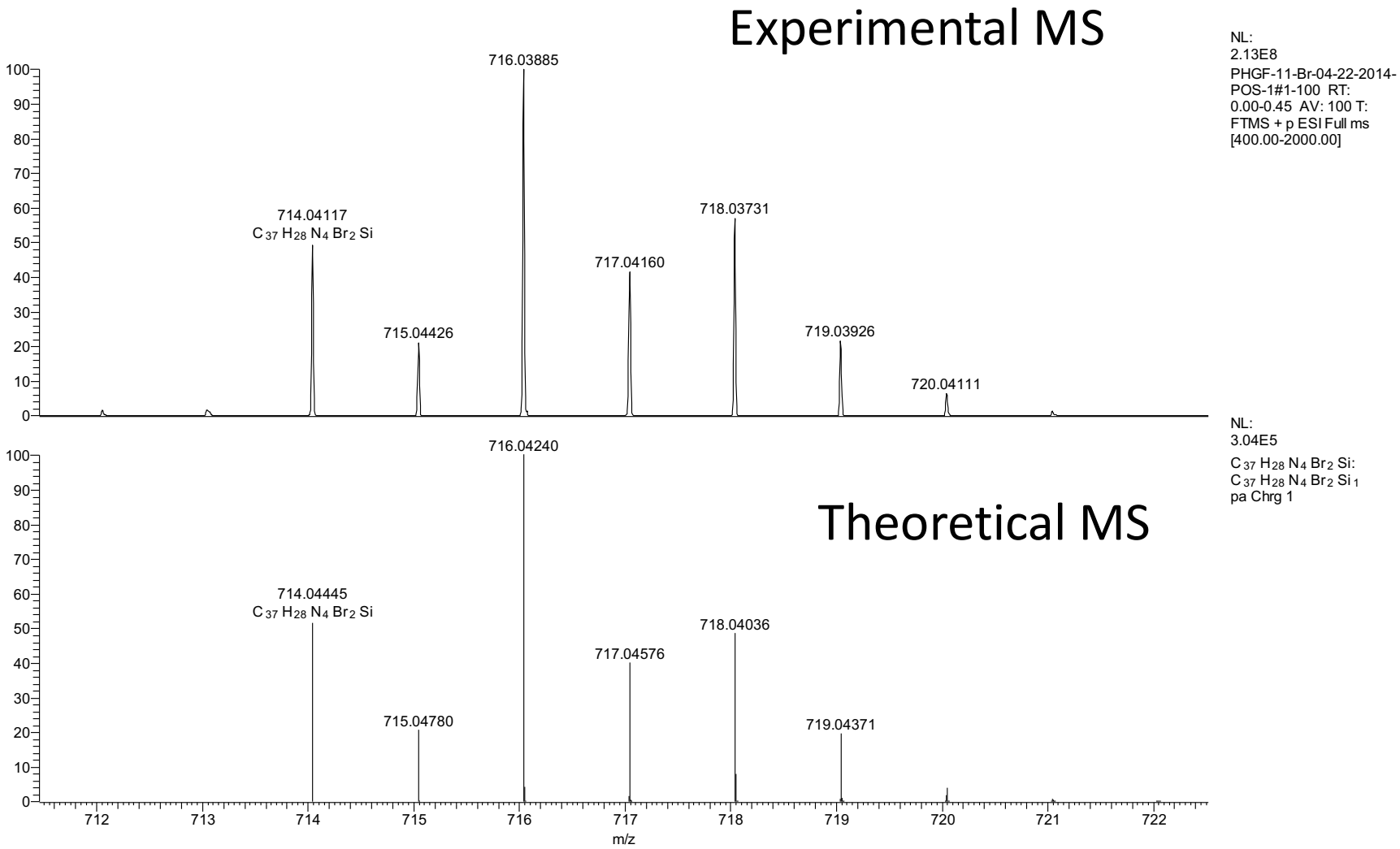

Figure S10. The ESI-MS spectrum of **2-Br$_2$/TMS**.

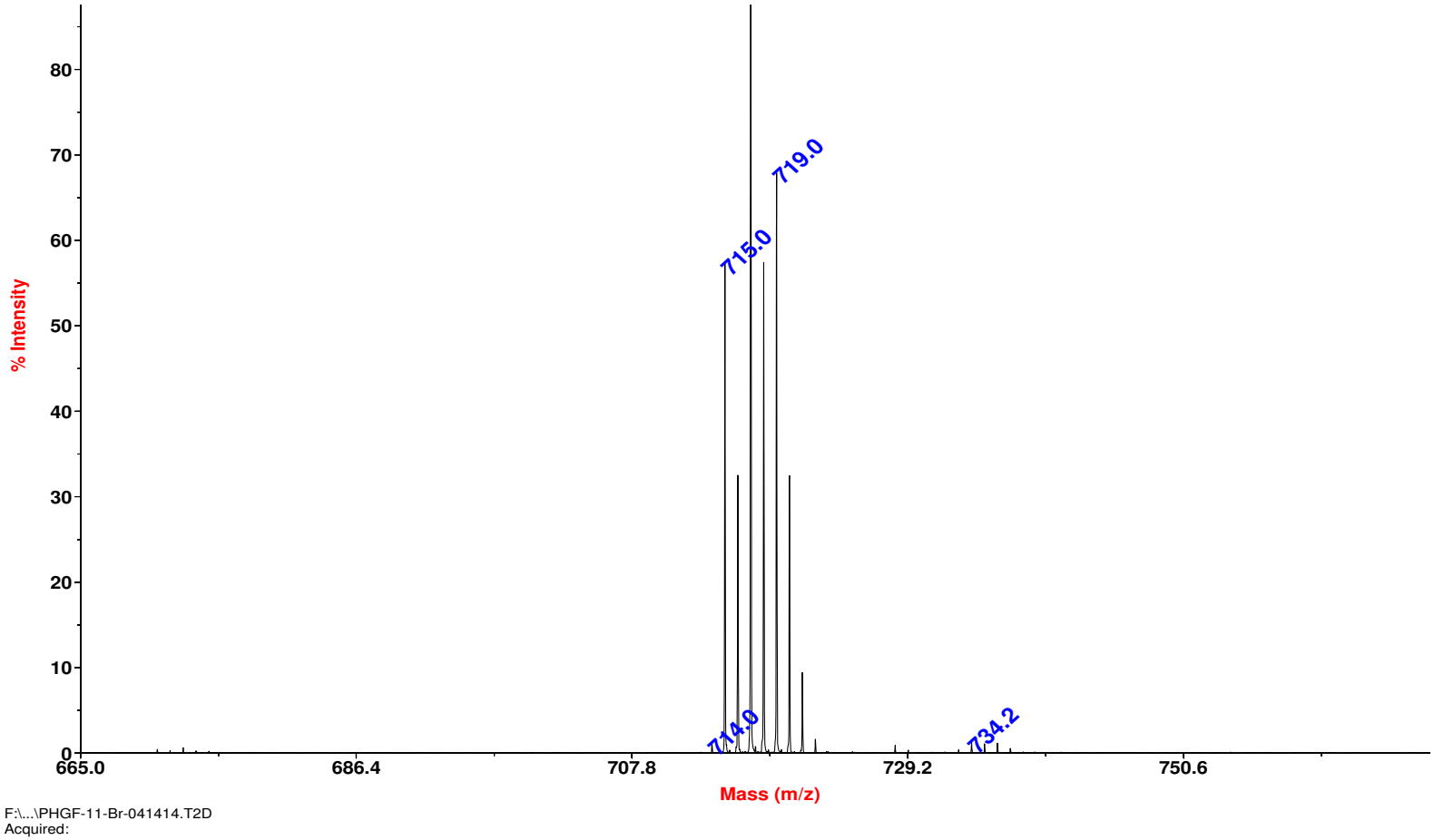

Figure S11. The MALDI-MS spectrum of **2-Br$_2$/TMS**.

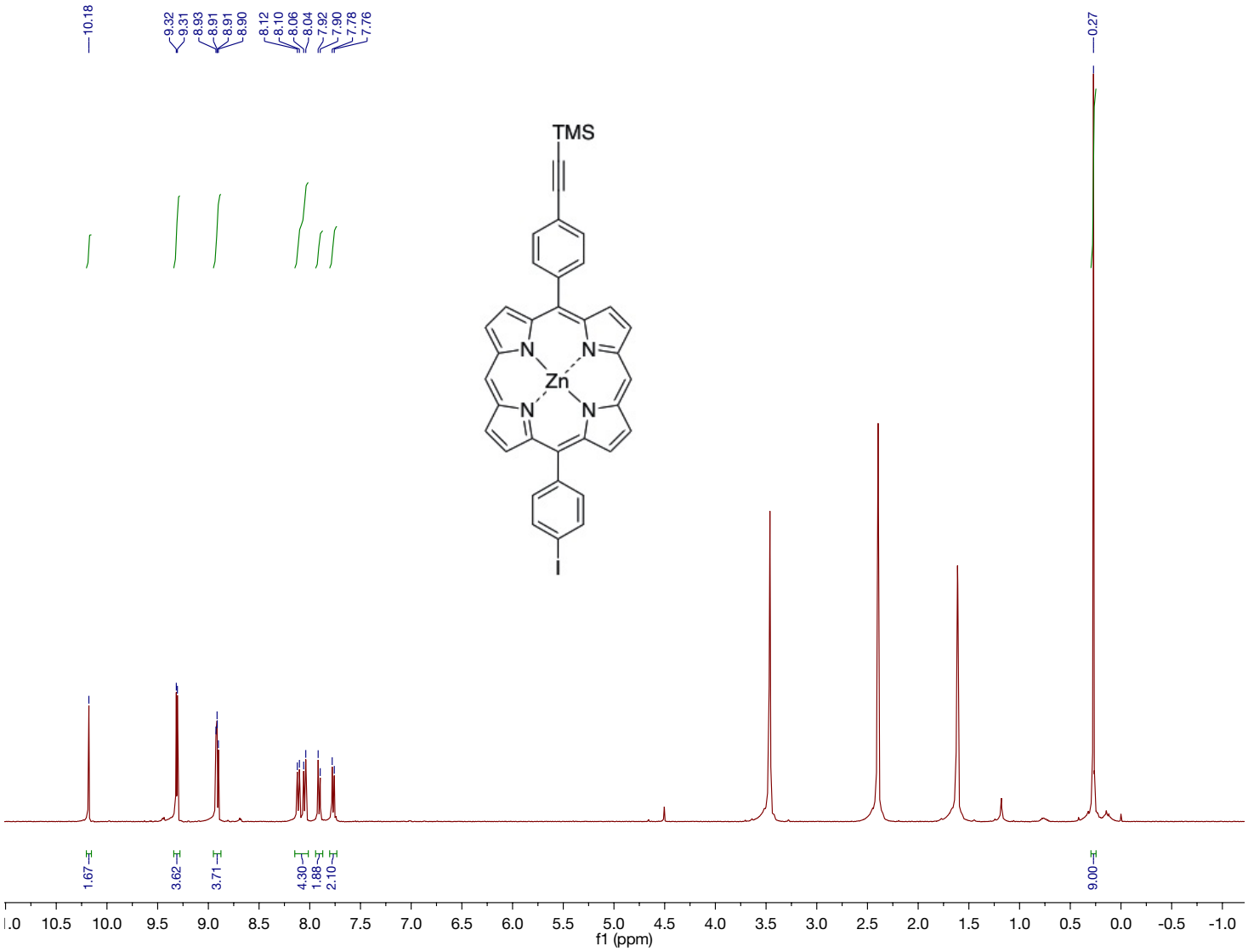

Figure S12. The ^{1}H NMR spectrum of **Zn4-I/TMS**.

MS Data

ZnP-TMS5I15 Experimental and Theoretical Isotopic Distribution for $C_{37}H_{27}IN_4SiZn$, $[M+H]^+$

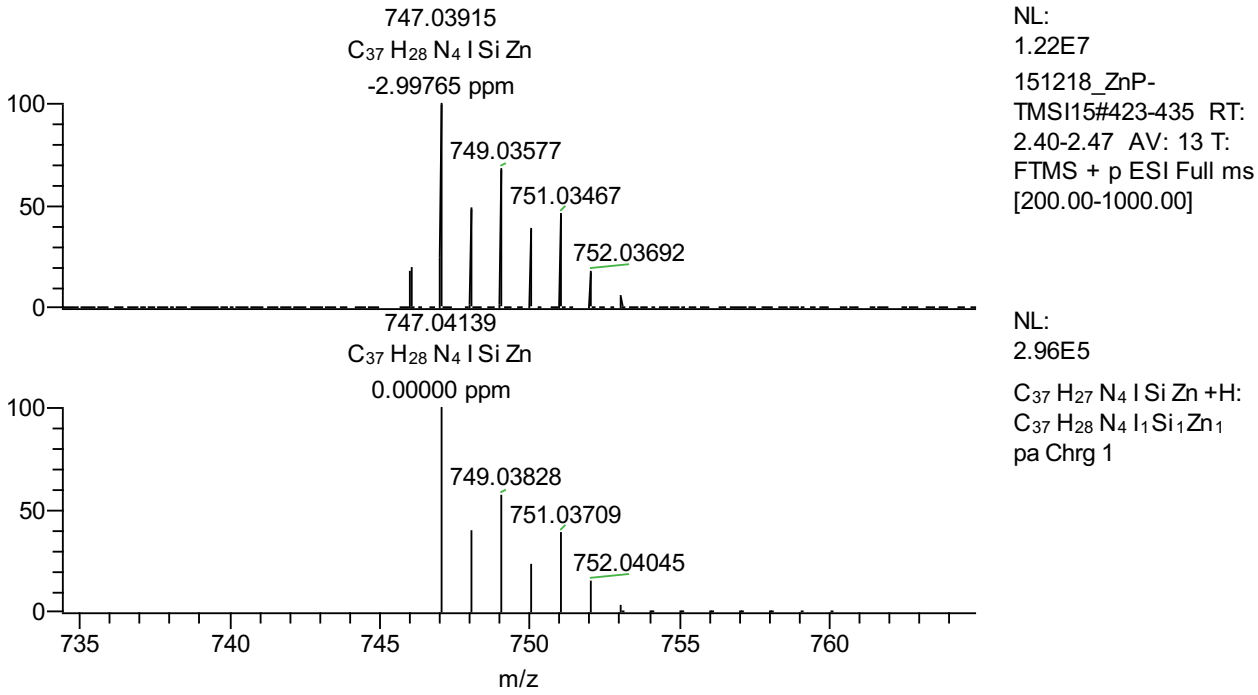

Figure S13. The ESI-MS spectrum of **Zn4-I/TMS**.

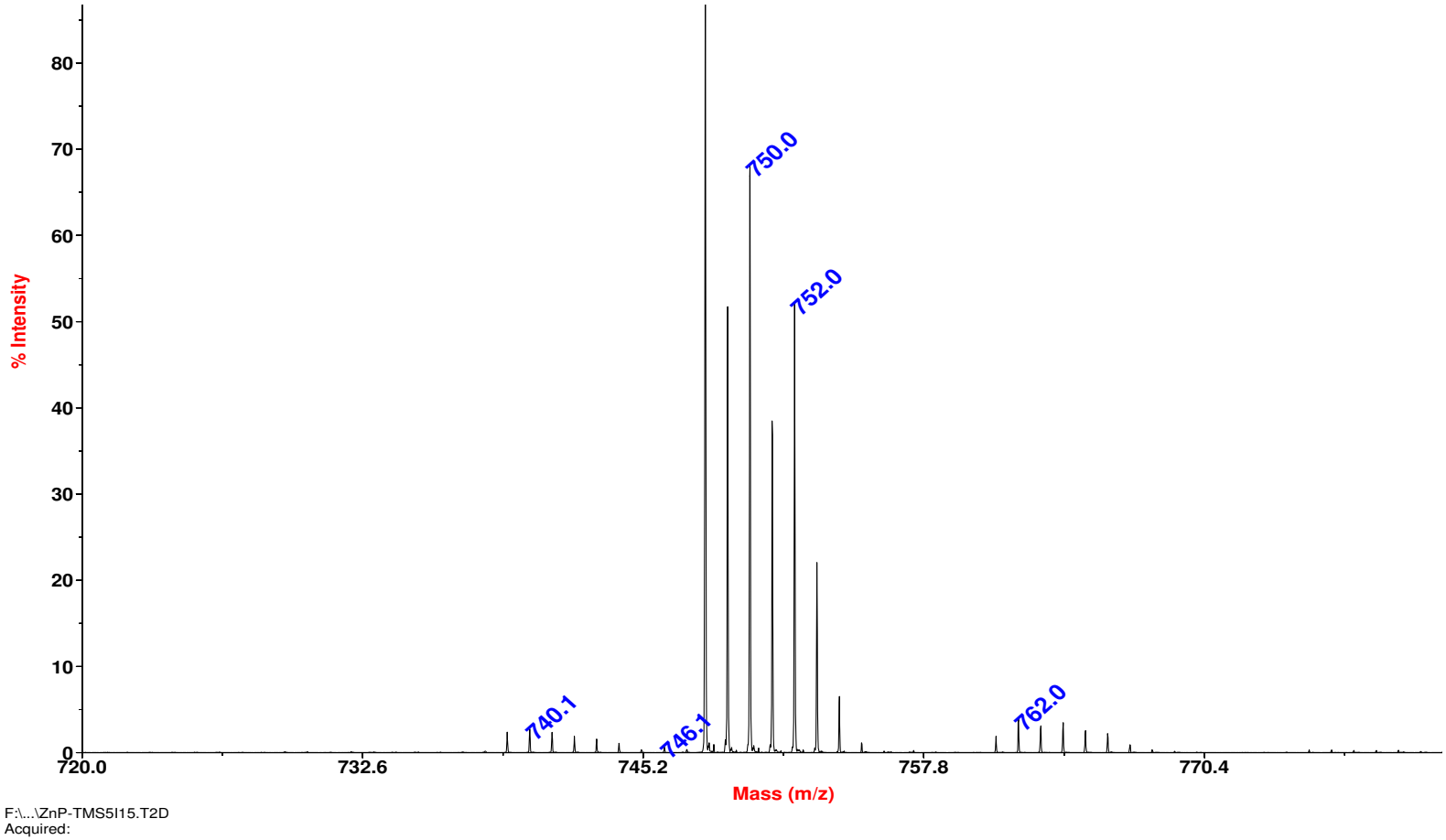

Figure S14. The MALDI-MS spectrum of **Zn4-I/TMS**.

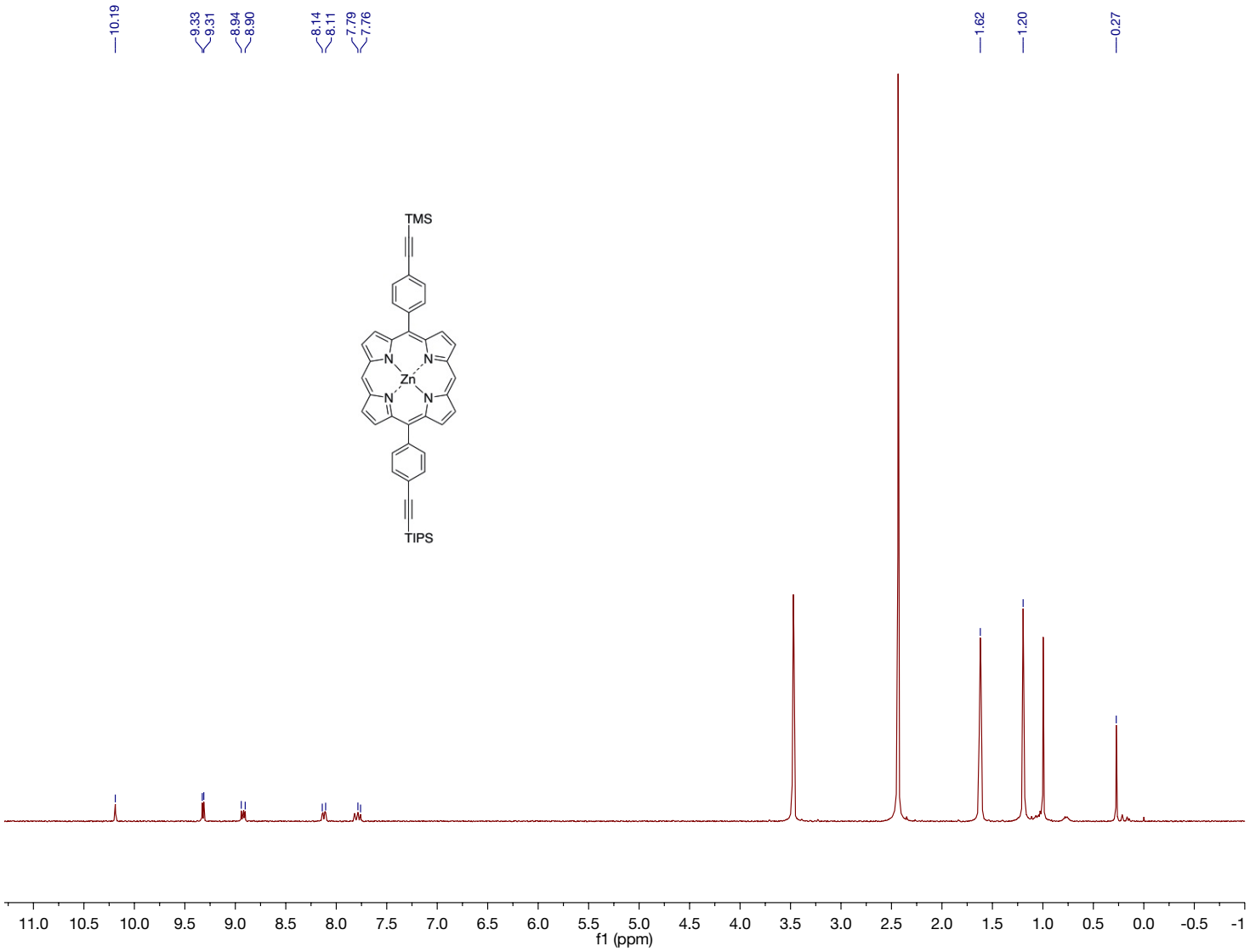

Figure S15. The ^{1}H NMR spectrum of **Zn4-TMS/TIPS**.

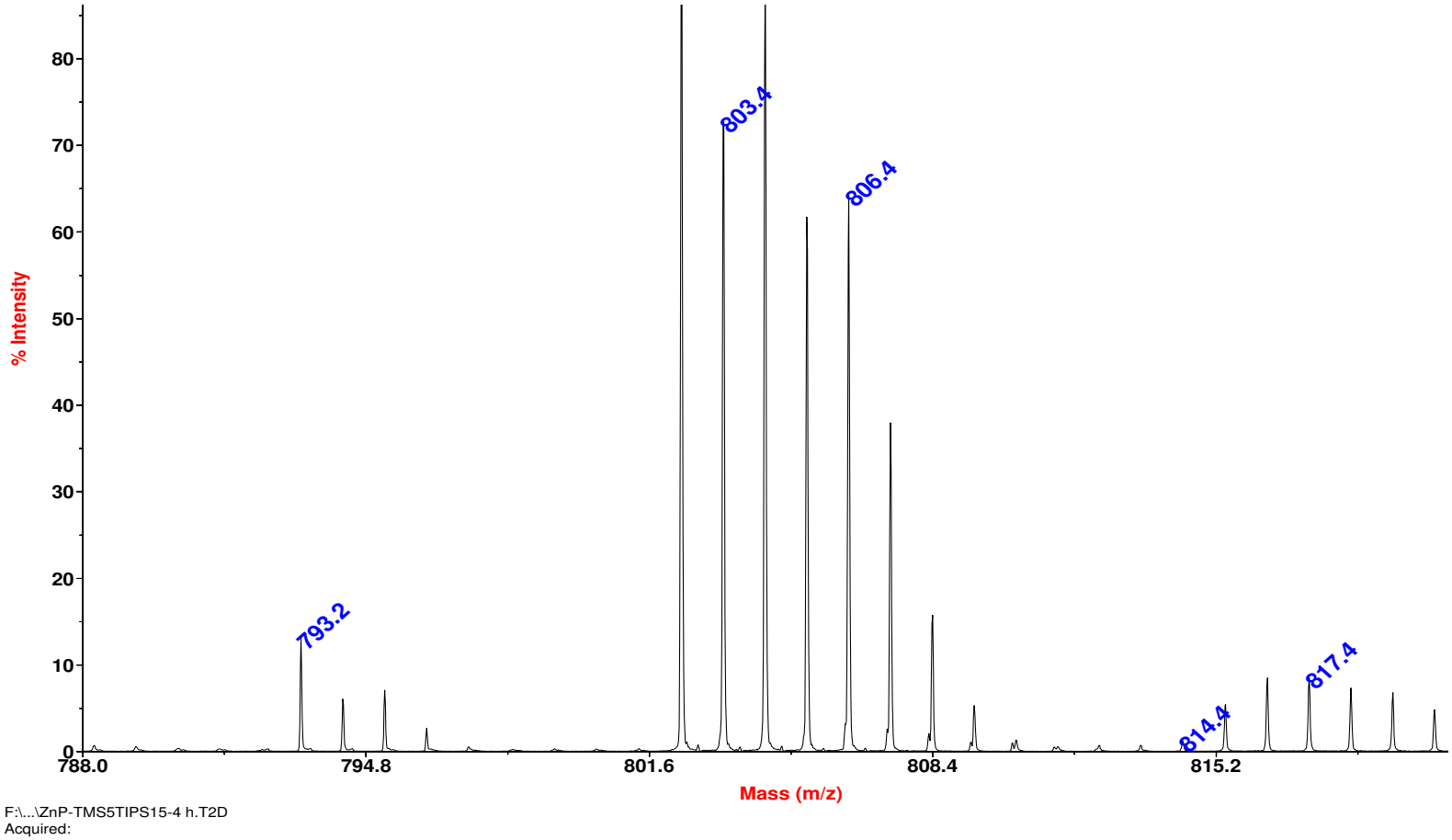

Figure S16. The MALDI-MS spectrum of **Zn4-TMS/TIPS**.

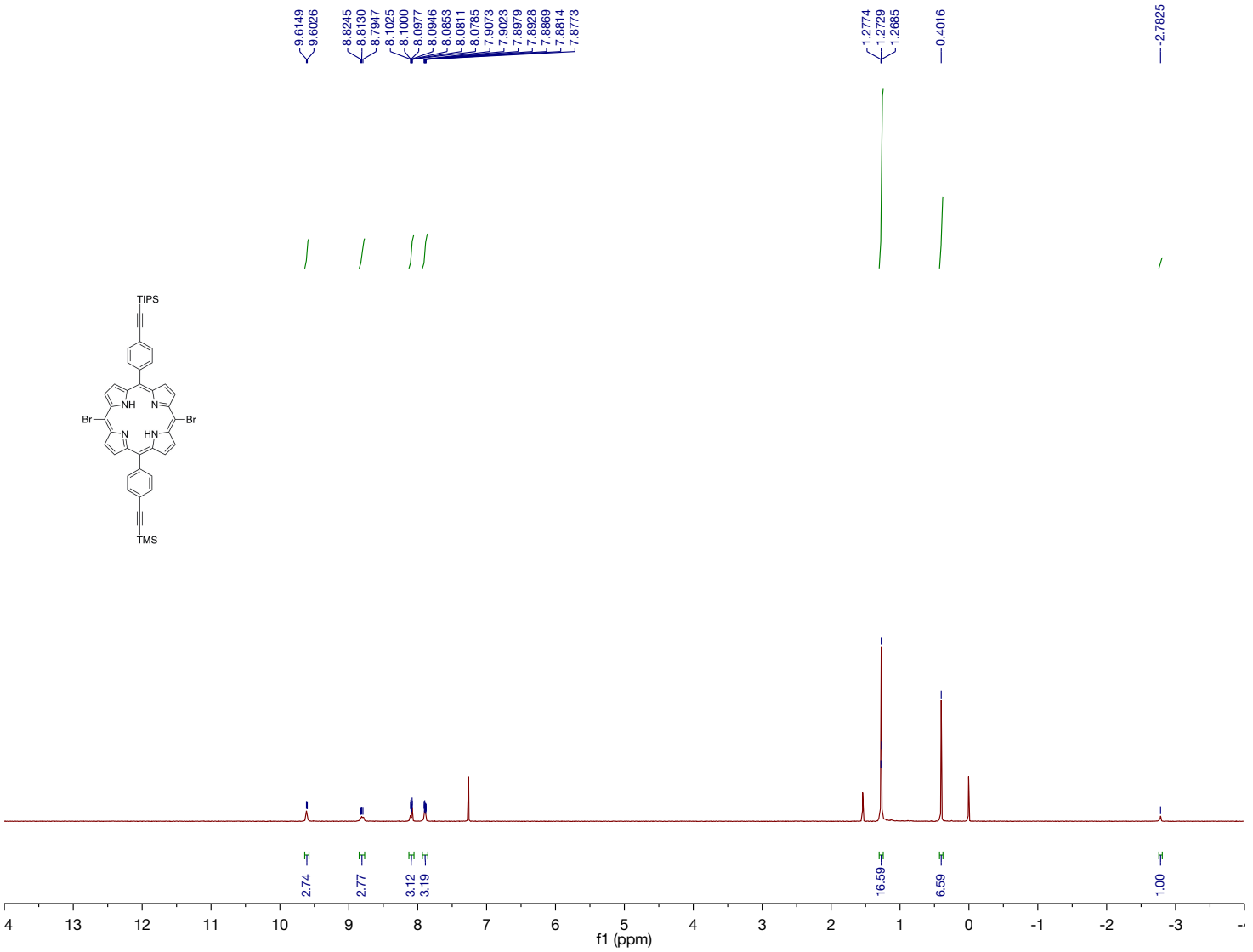

Figure S17. The ^{1}H NMR spectrum of **4-Br$_2$/TMS/TIPS**.

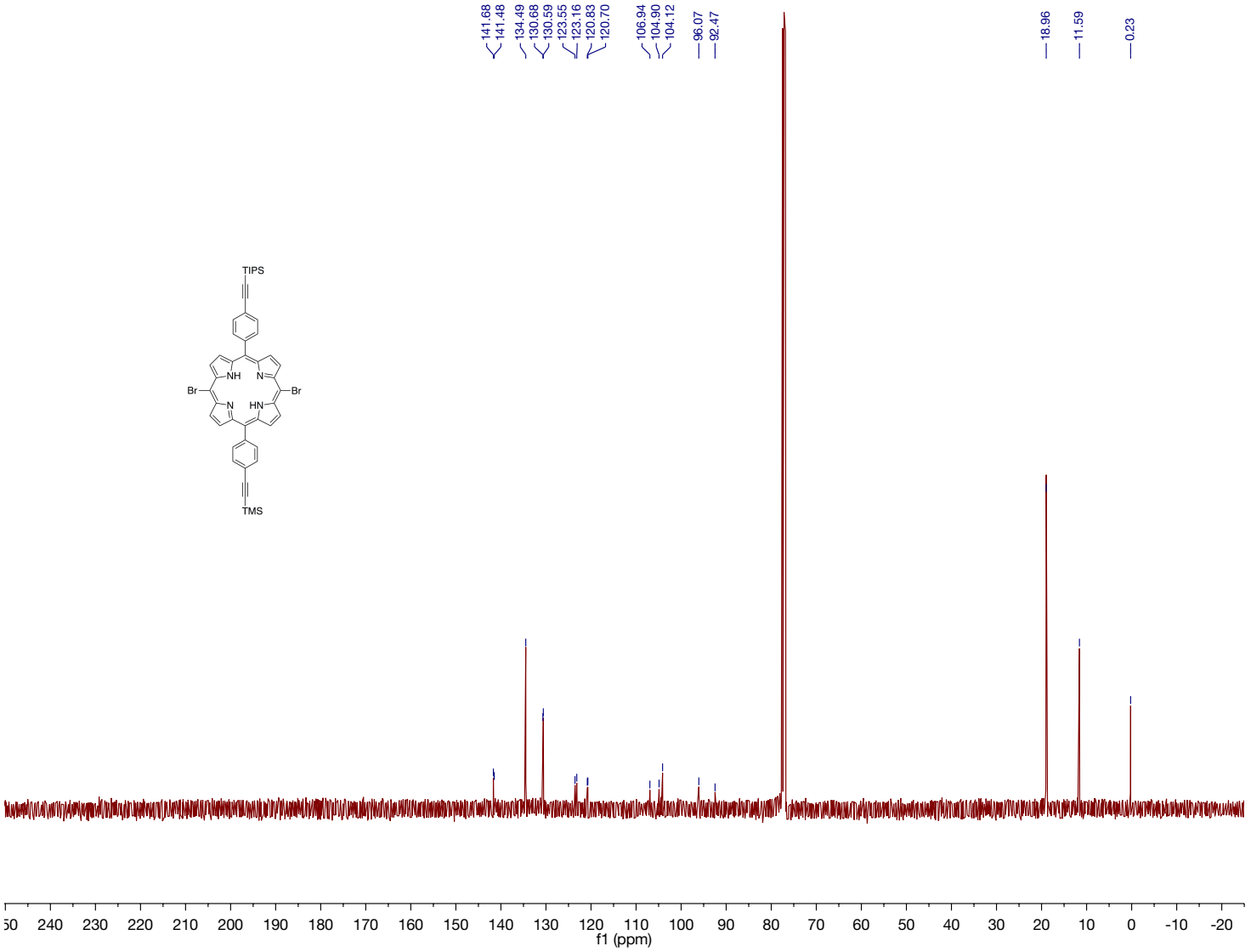

Figure S18. The ^{13}C NMR spectrum of **4-Br$_2$/TMS/TIPS**.

Sample	$M_{Theoretical}$	$M_{Experimental}$	ΔM (ppm)	Elemental Composition
FbP-TMS5TIPS15Br2	895.18570 $[M]^+$	895.18357 $[M]^+$	-2.386	$C_{48}H_{49}Br_2N_4Si_2$

MS Data

FbP-TMS5TIPS15Br2 Experimental and Theoretical Isotopic Distribution for $C_{48}H_{49}Br_2N_4Si_2$, $[M+H]^+$

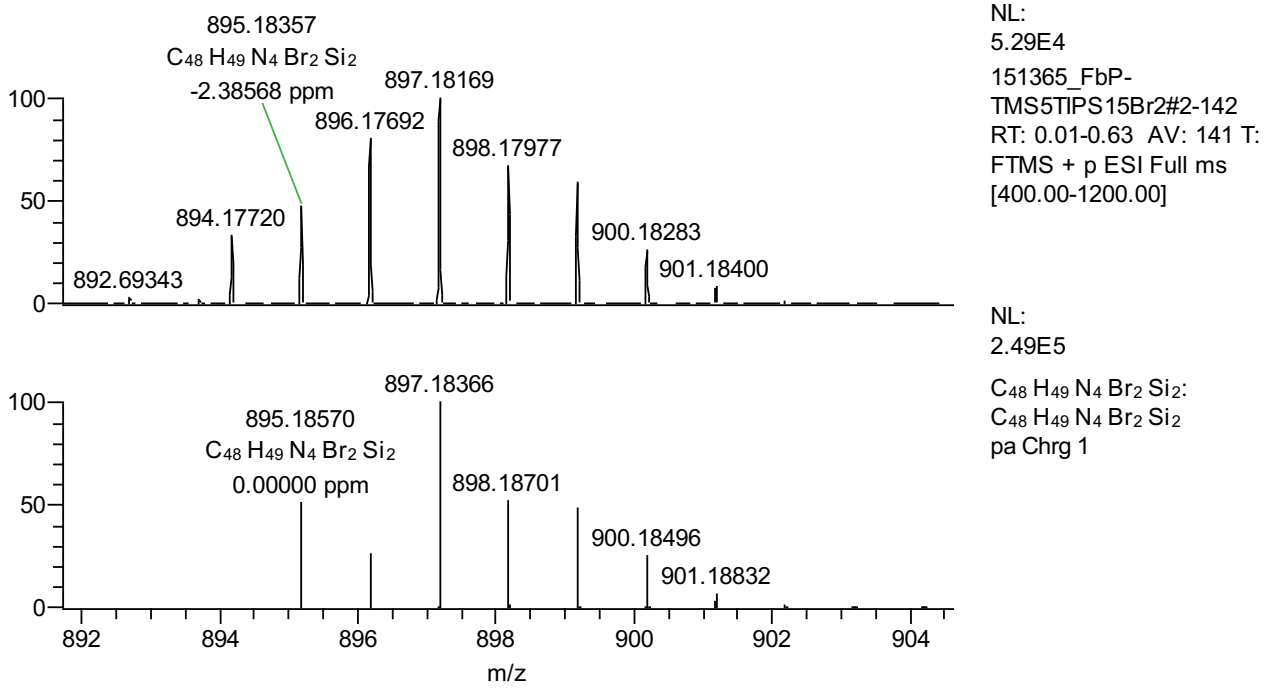

Figure S19. The ESI-MS spectrum of **4-Br_2/TMS/TIPS**.

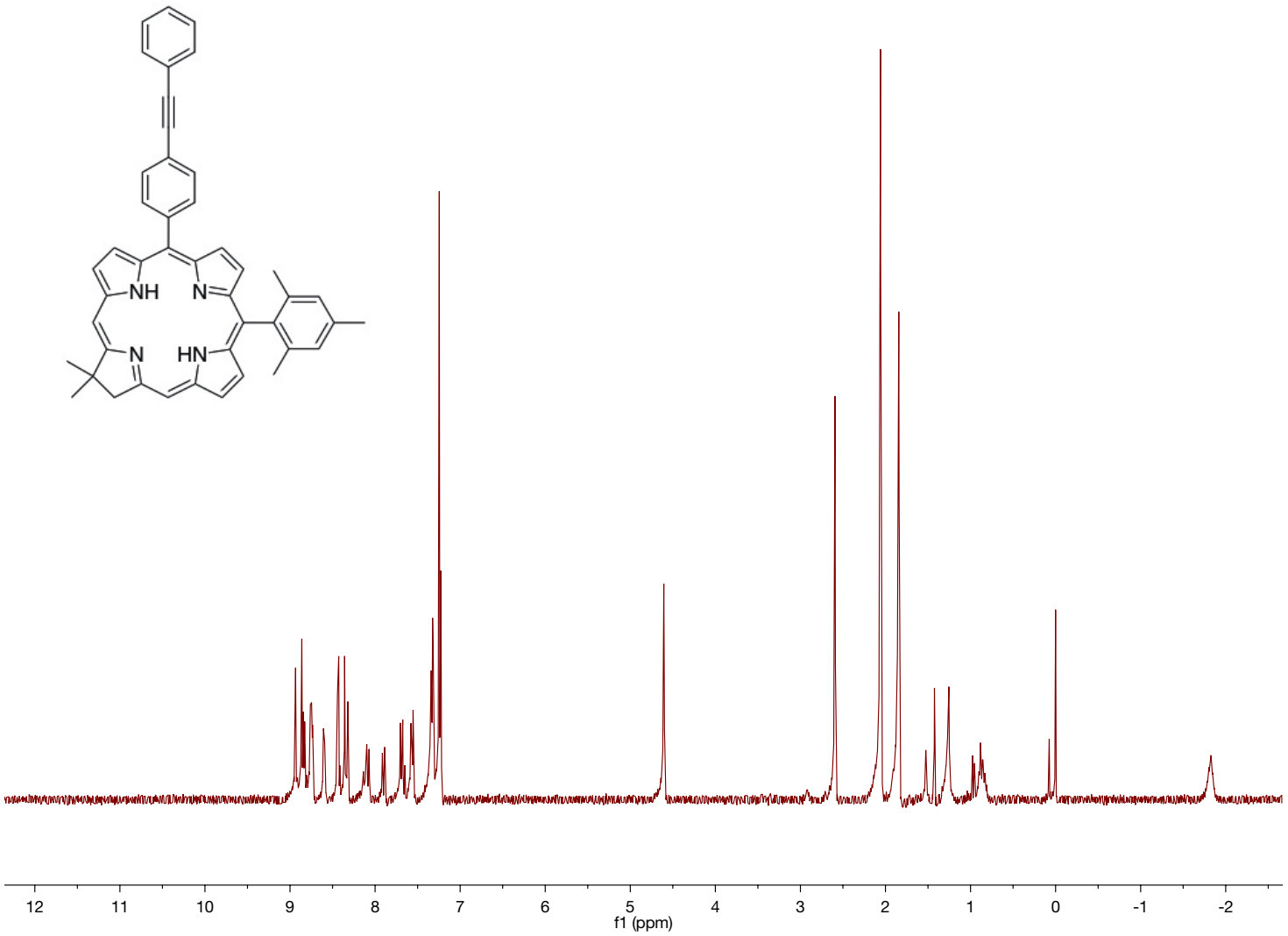

Figure S20. The ^{1}H NMR spectrum of **C-Ph**.

Sample	$M_{Theoretical}$	$M_{Experimental}$	ΔM (ppm)	Elemental Composition
FbC-pep	635.31692 $[M+H]^+$	635.31711 $[M+H]^+$	0.287	$C_{45}H_{38}N_4$

MS Data

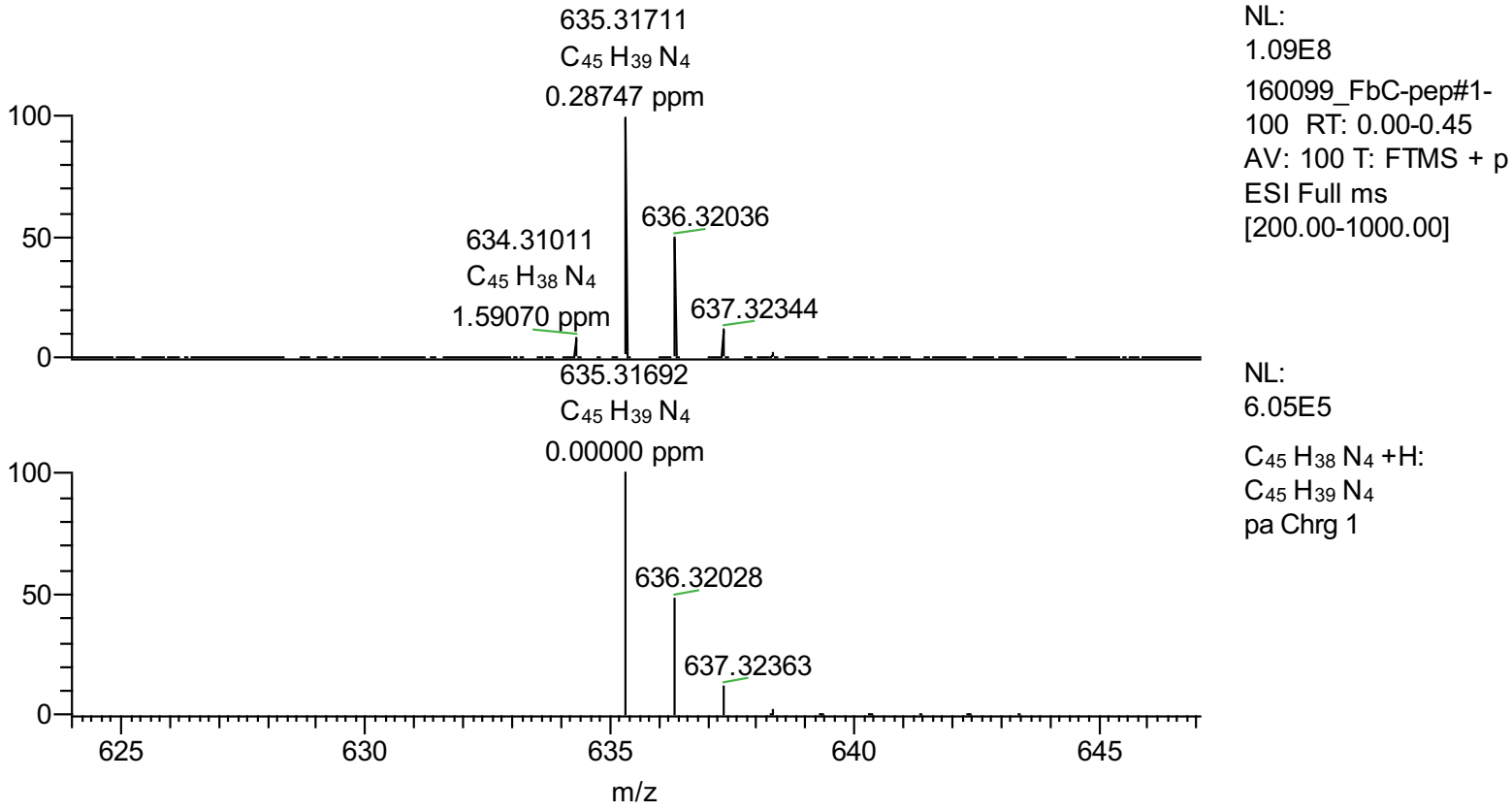

Figure S21. The ESI-MS spectrum of **C-Ph**.

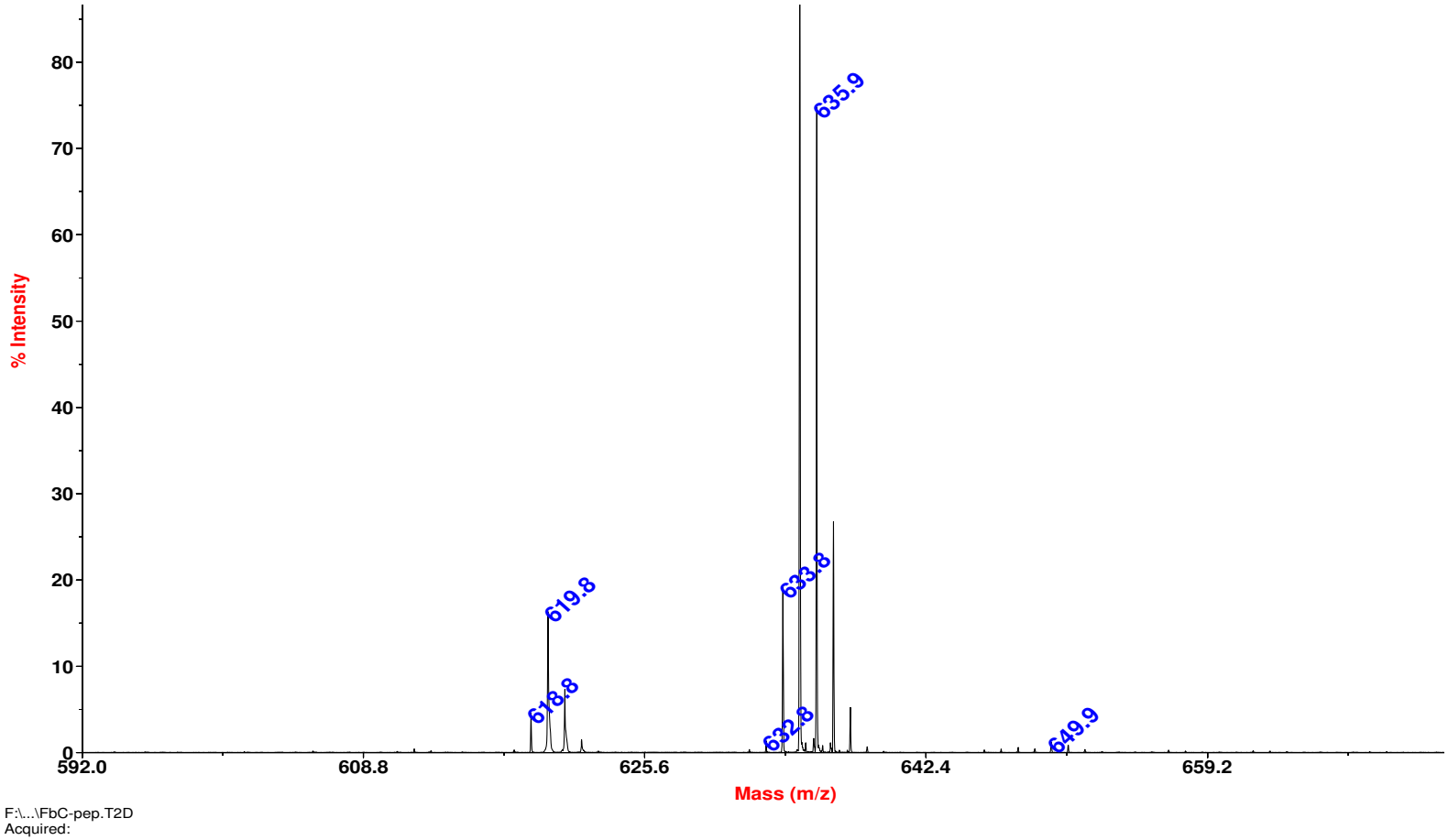

Figure S22. The MALDI-MS spectrum of **C-Ph**.

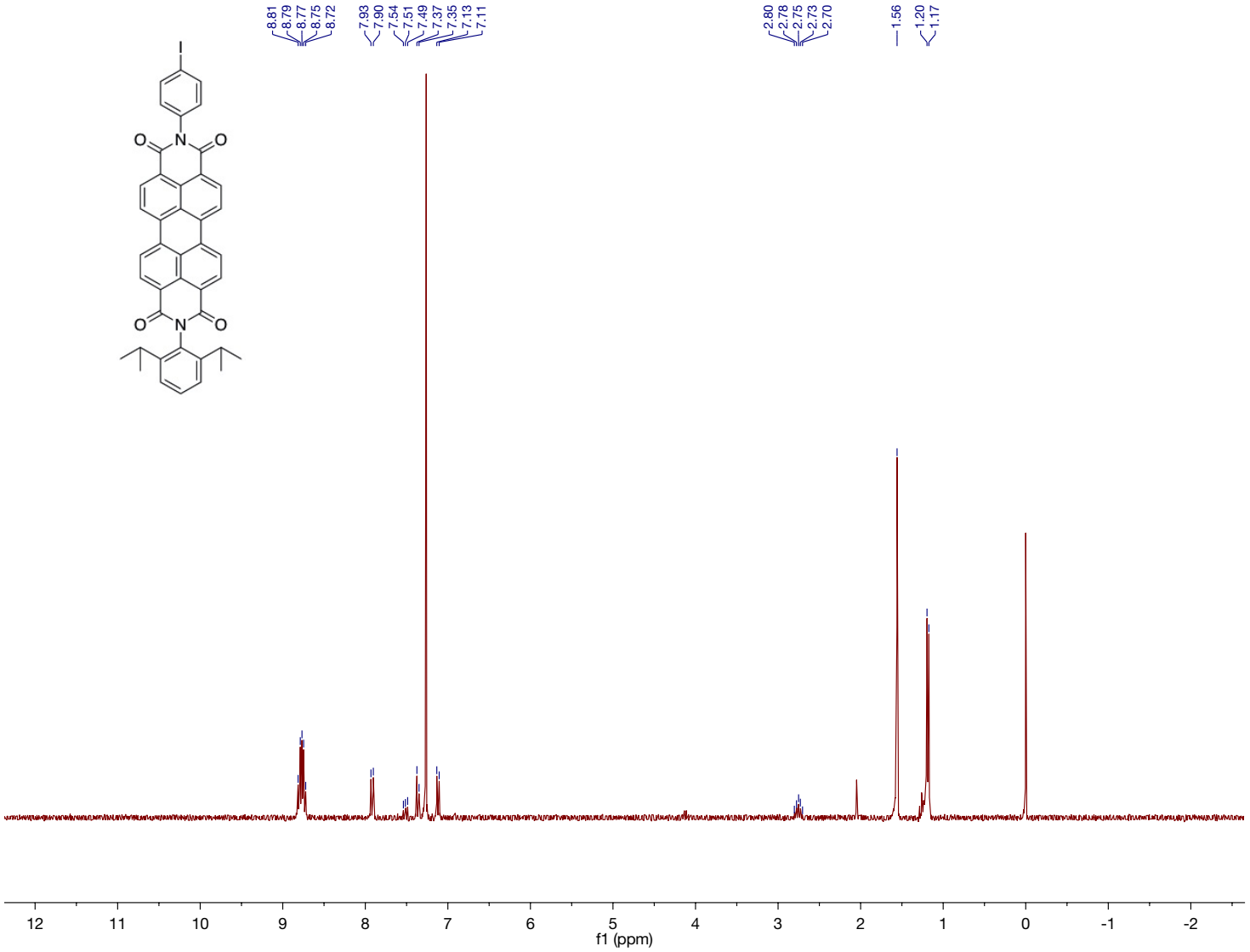

Figure S23. The ^{1}H NMR spectrum of **7**.

Sample	$M_{Theoretical}$	$M_{Experimental}$	ΔM (ppm)	Elemental Composition
PDI-I	753.12448 $[M+H]^+$	753.12351 $[M+H]^+$	-1.283	$C_{42}H_{29}IN_2O_4$

MS Data

PDI-I Experimental and Theoretical Isotopic Distribution, $C_{42}H_{29}IN_2O_4$, $[M]^+$ and $[M+H]^+$

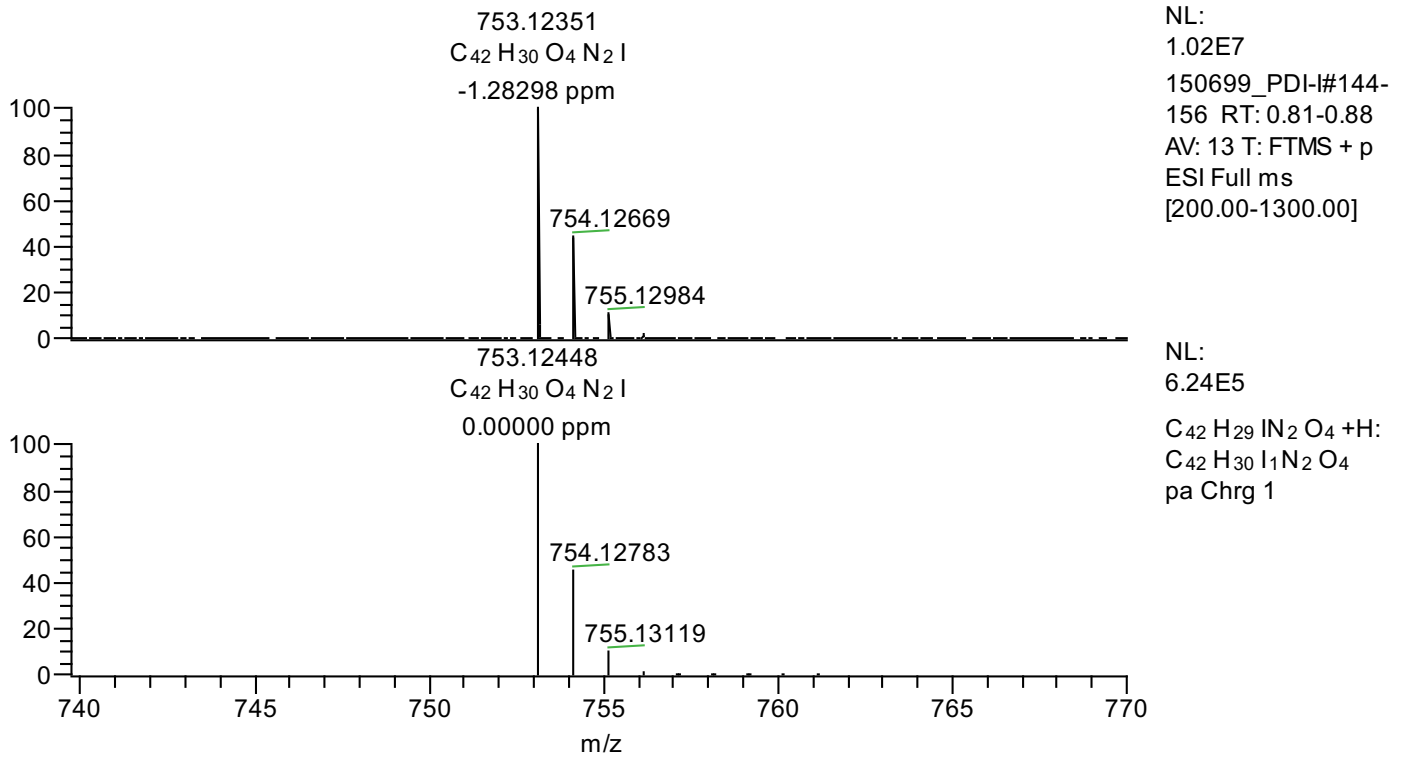

Figure S24. The ESI-MS spectrum of **7**.

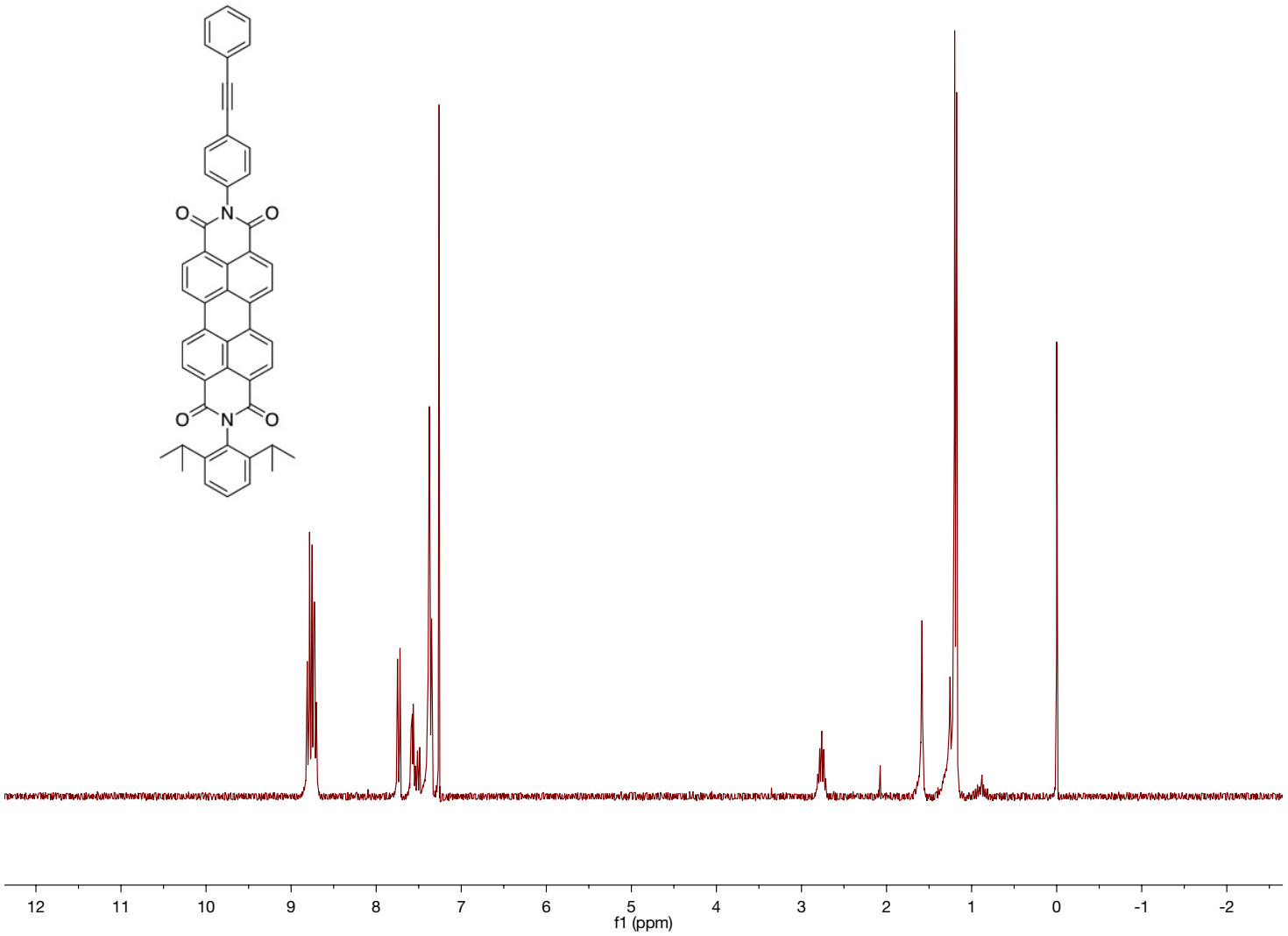

Figure S25. The ^{1}H NMR spectrum of **PDI-Ph**.

Sample	$M_{Theoretical}$	$M_{Experimental}$	ΔM (ppm)	Elemental Composition
PDI	727.25913 $[M+H]^+$	727.25526 $[M+H]^+$	-1.204	$C_{50}H_{34}N_2O_4$

MS Data

PDI Experimental and Theoretical Isotopic Distribution for $C_{50}H_{34}N_2O_4$, $[M+H]^+$

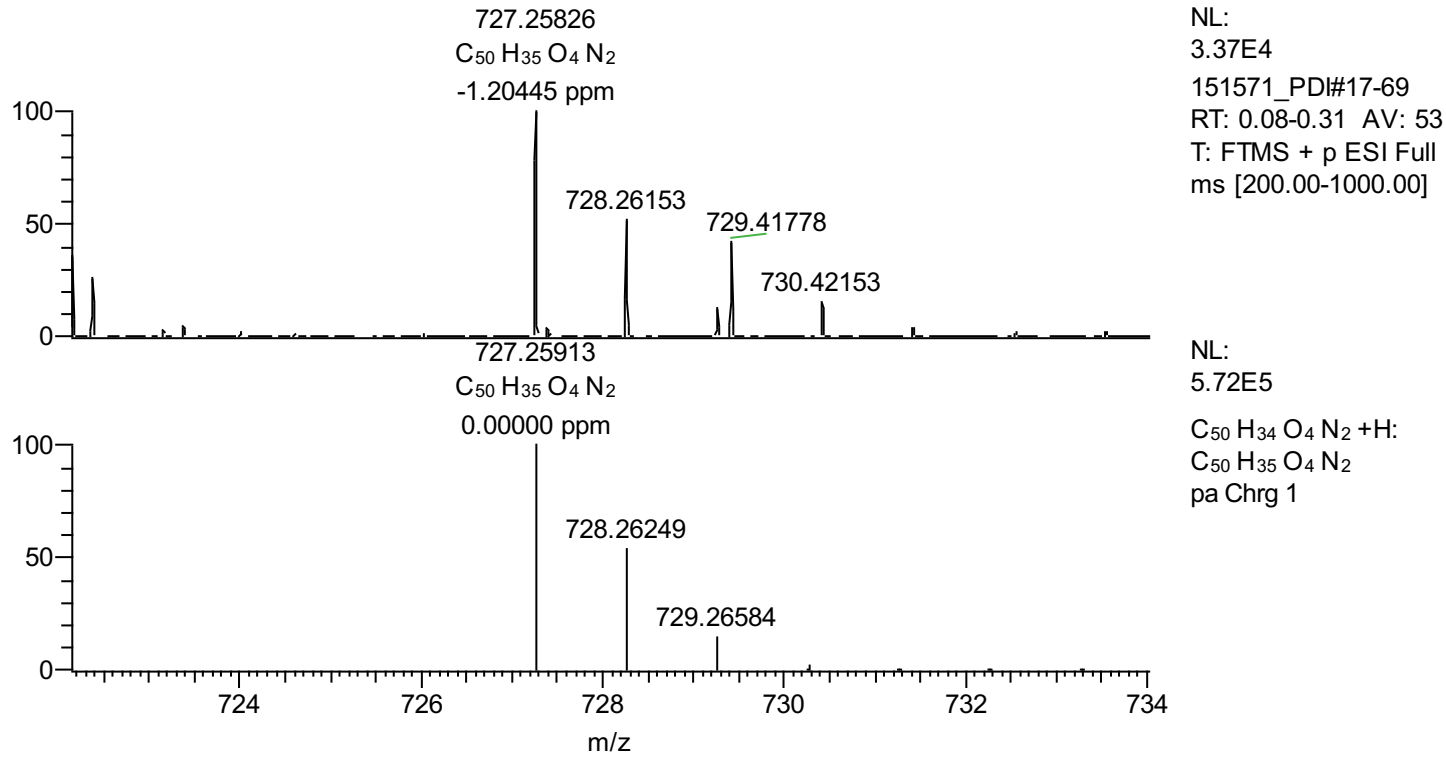

Figure S26. The ESI-MS spectrum of **PDI-Ph**.

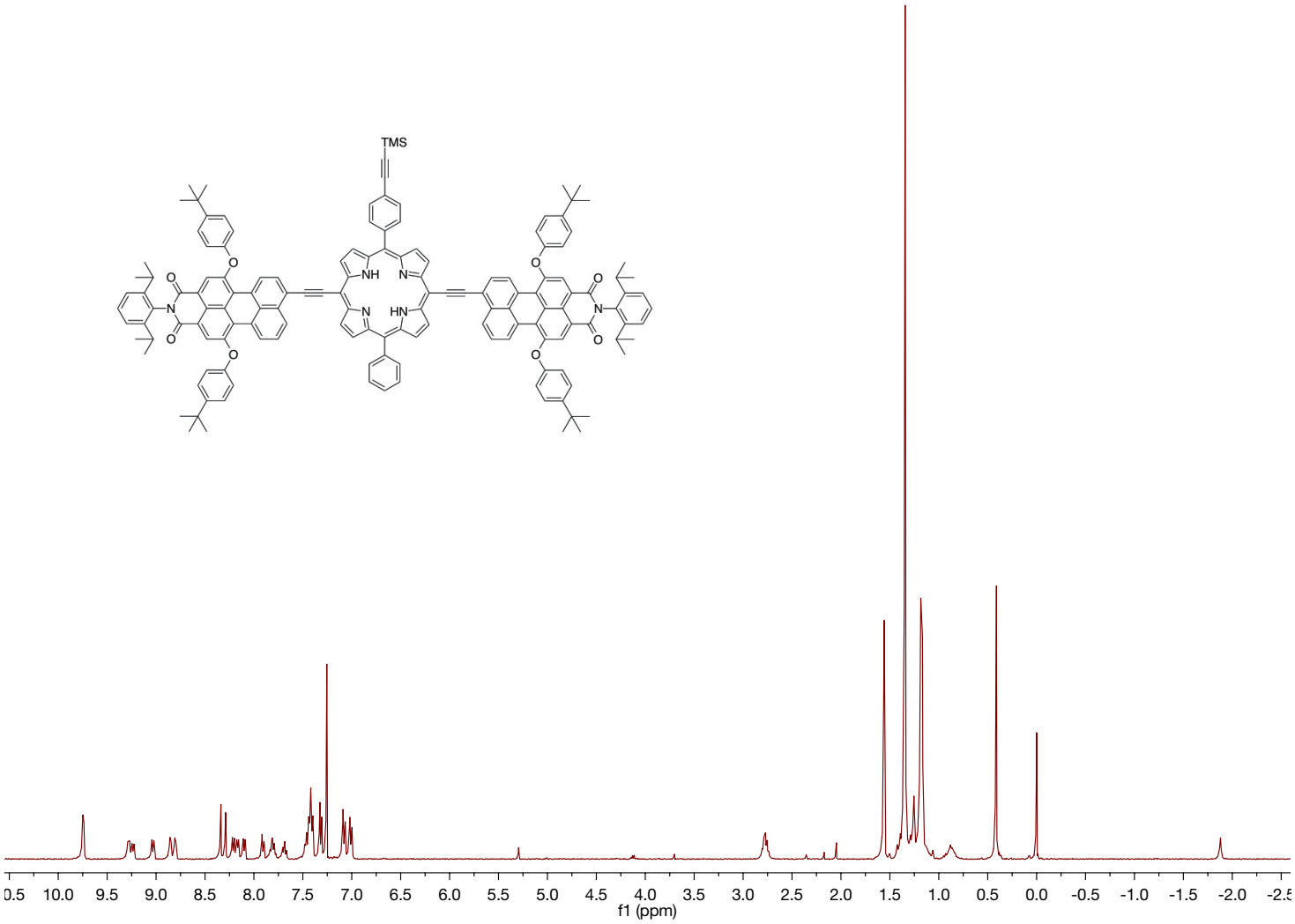

Figure S27. The ^{1}H NMR spectrum of **T-Ph**.

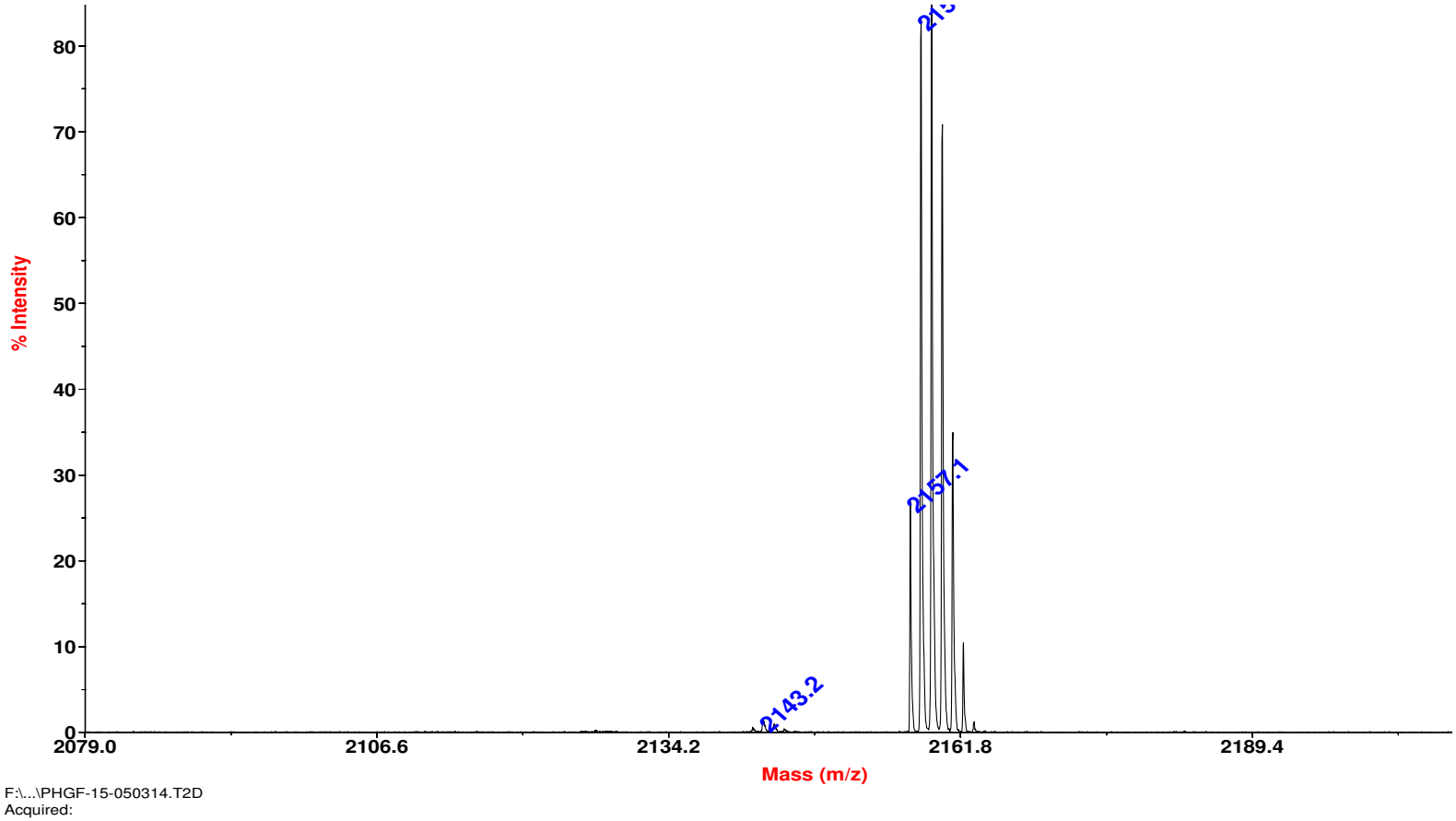

Figure S28. The MALDI-MS spectrum of **T-Ph**.

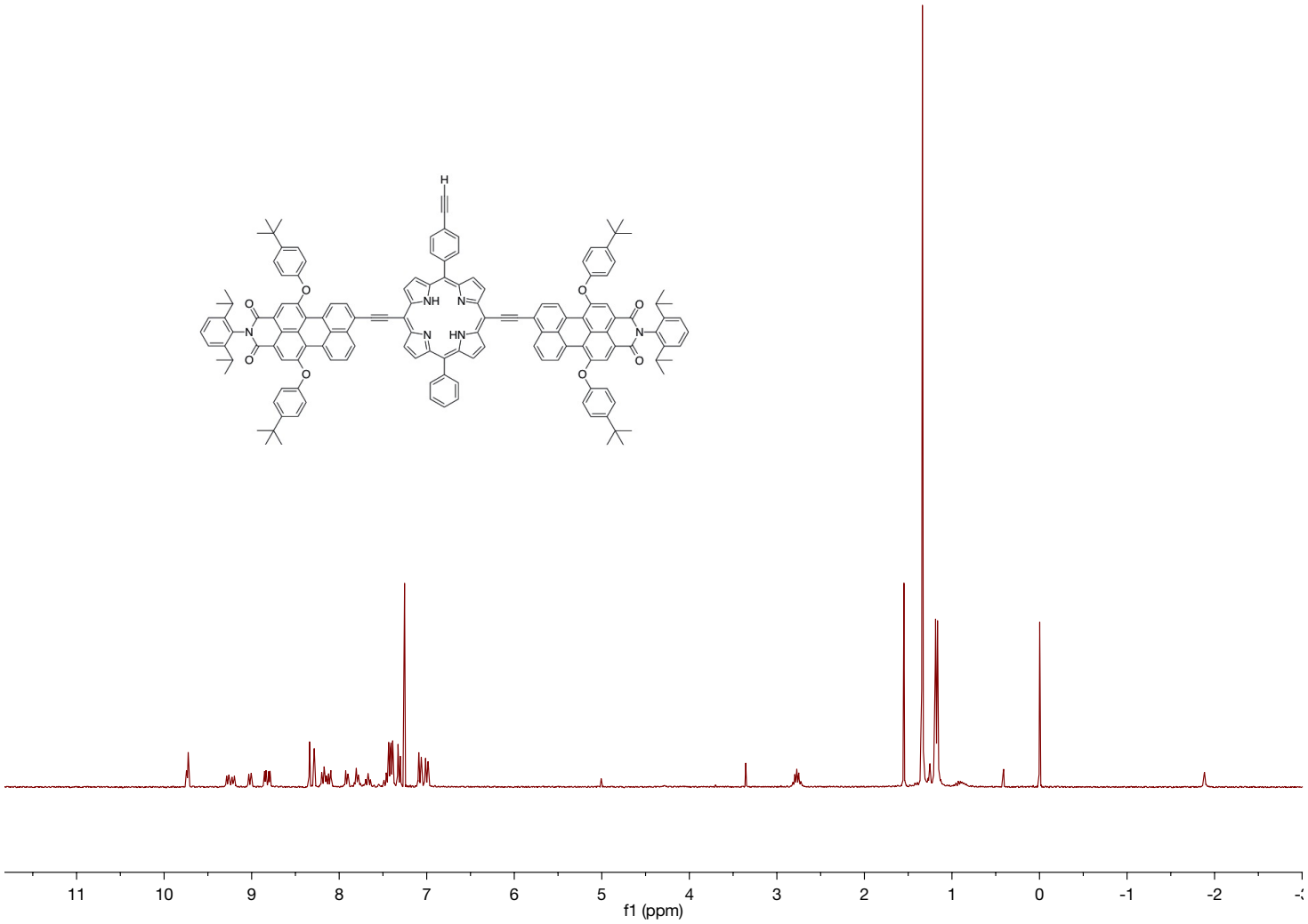

Figure S29. The ^{1}H NMR spectrum of **T-Ph-H**.

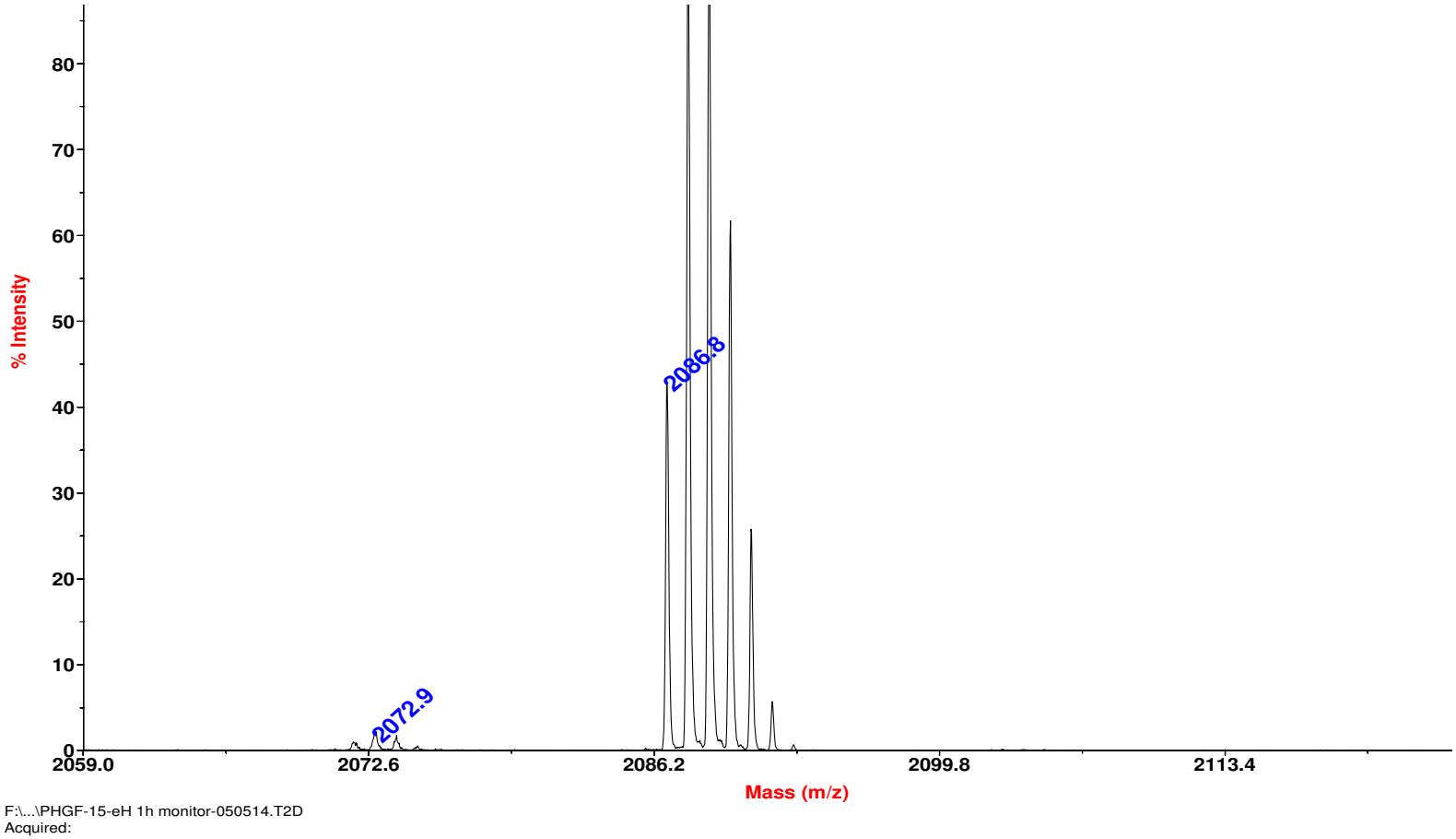

Figure S30. The MALDI-MS spectrum of **T-Ph-H**.

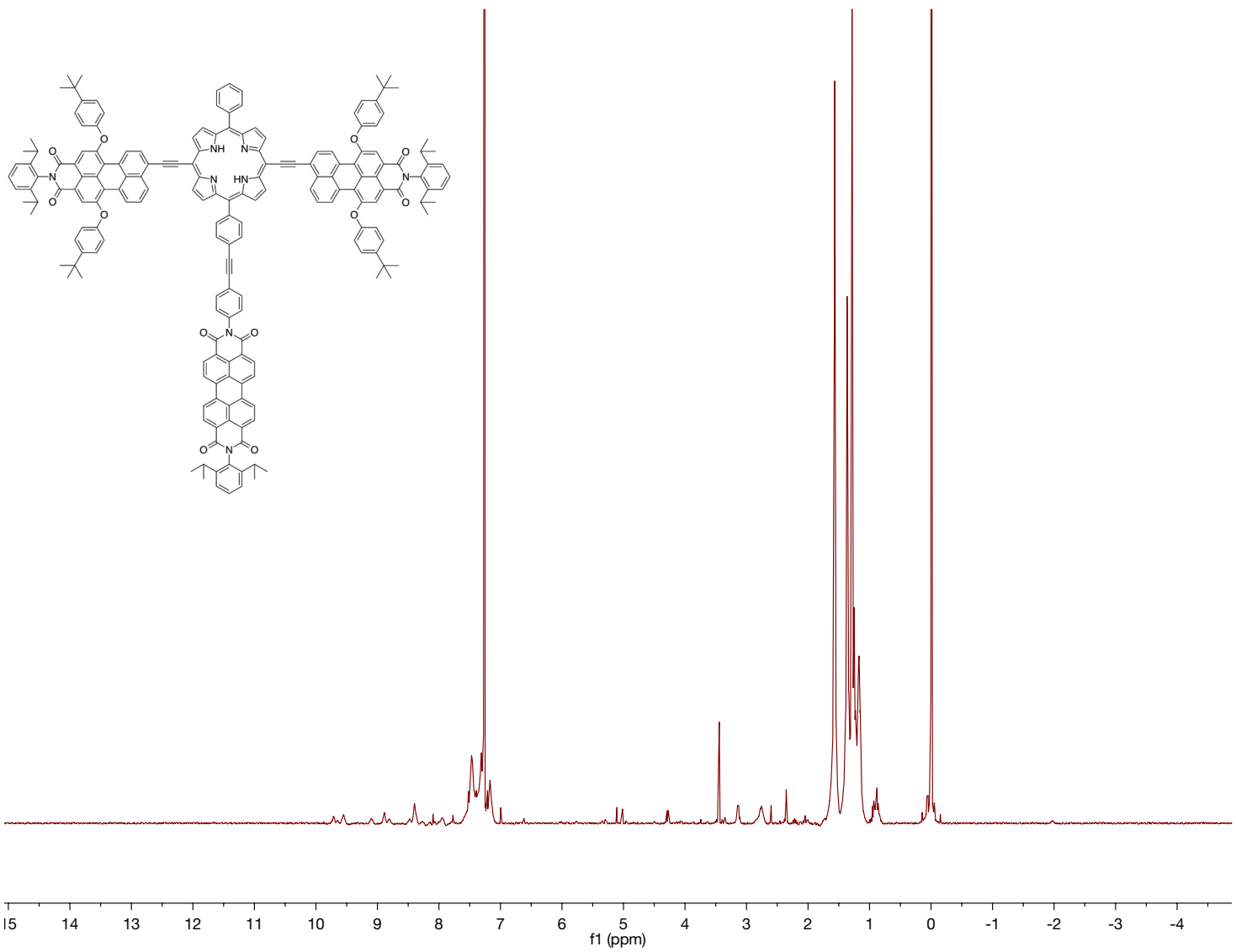

Figure S31. The ^{1}H NMR spectrum of **T-PDI**.

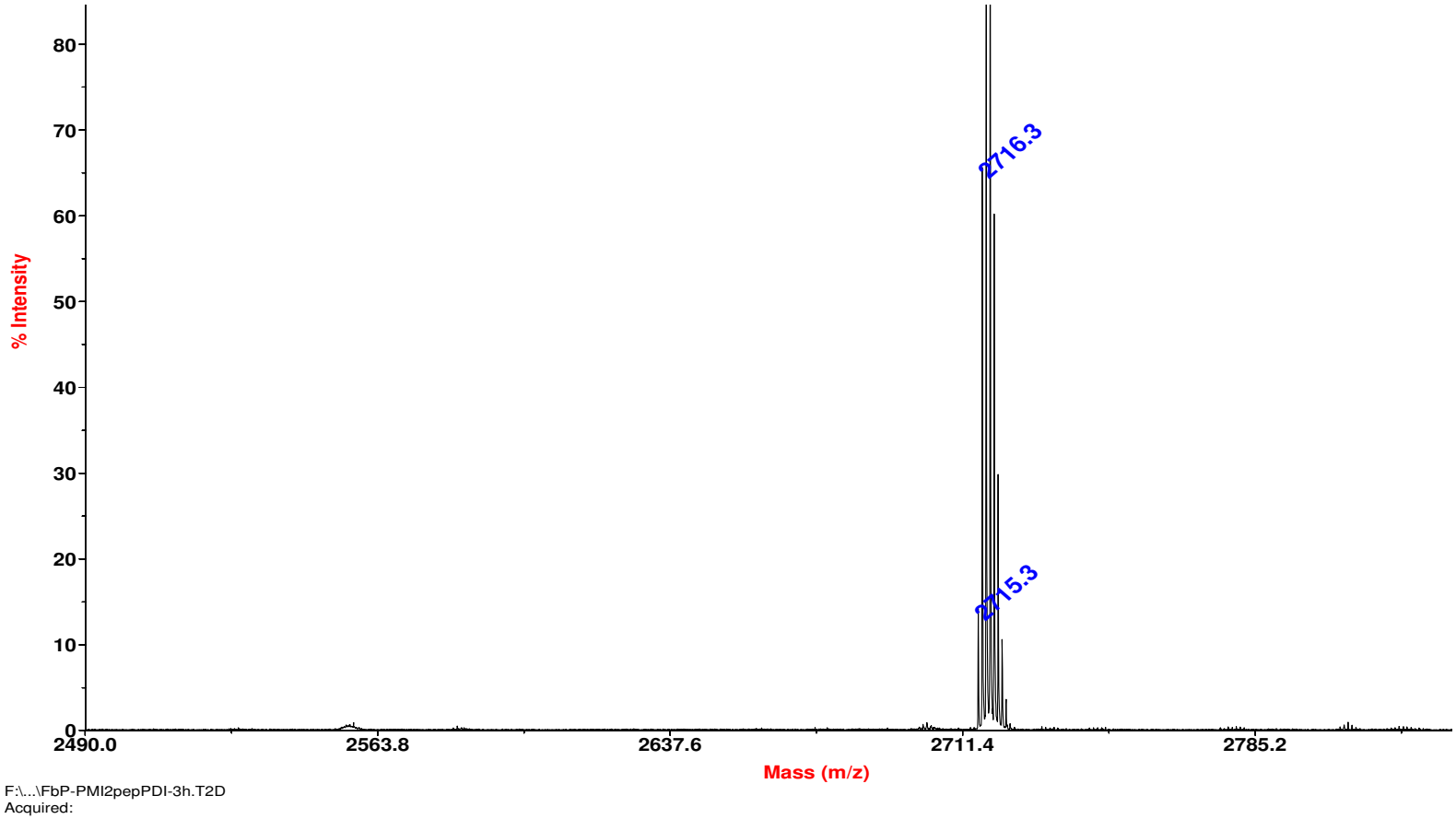

Figure S32. The MALDI-MS spectrum of **T-PDI**.

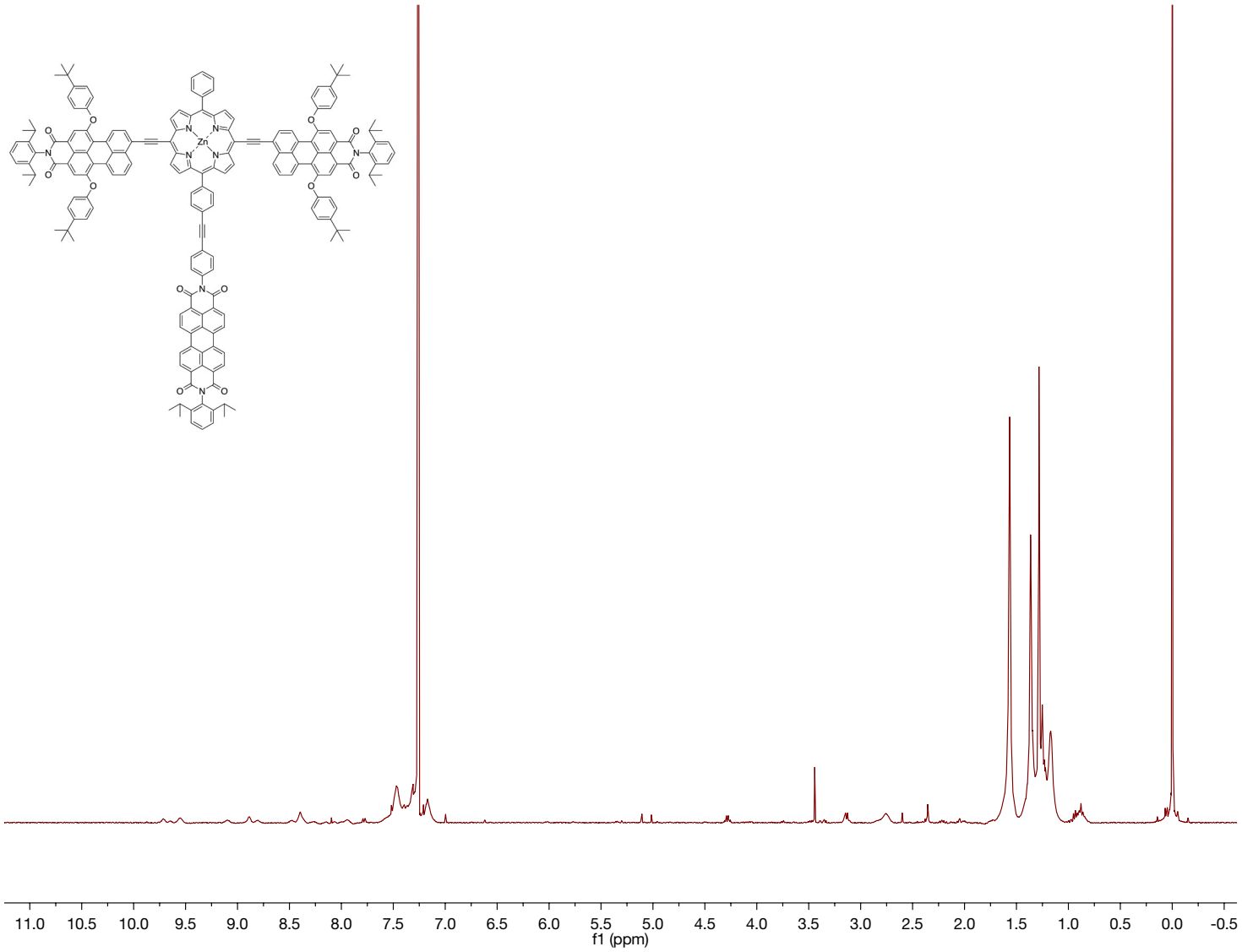

Figure S33. The ^{1}H NMR spectrum of **ZnT-PDI**.

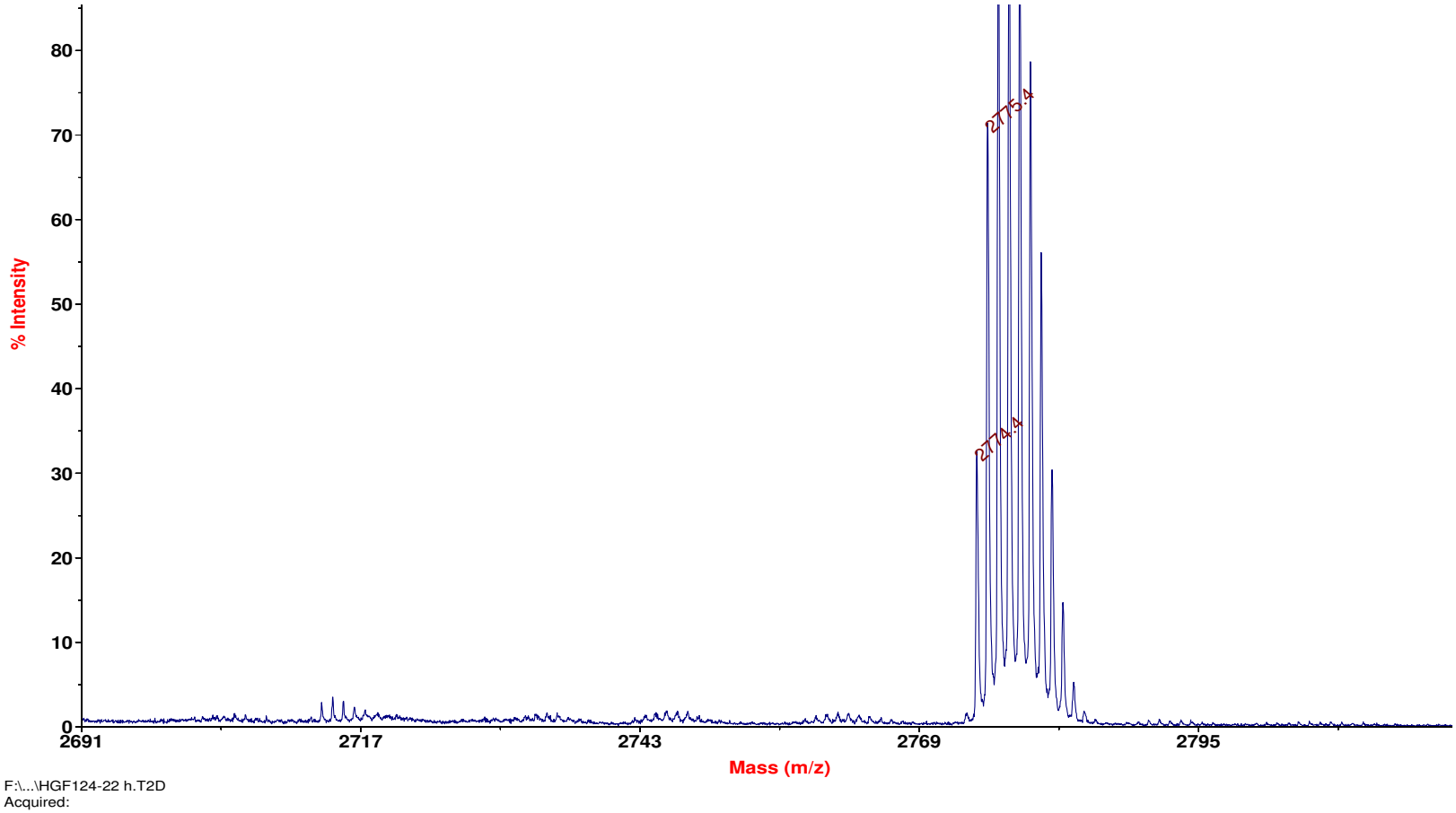

Figure S34. The MALDI-MS spectrum of **ZnT-PDI**.

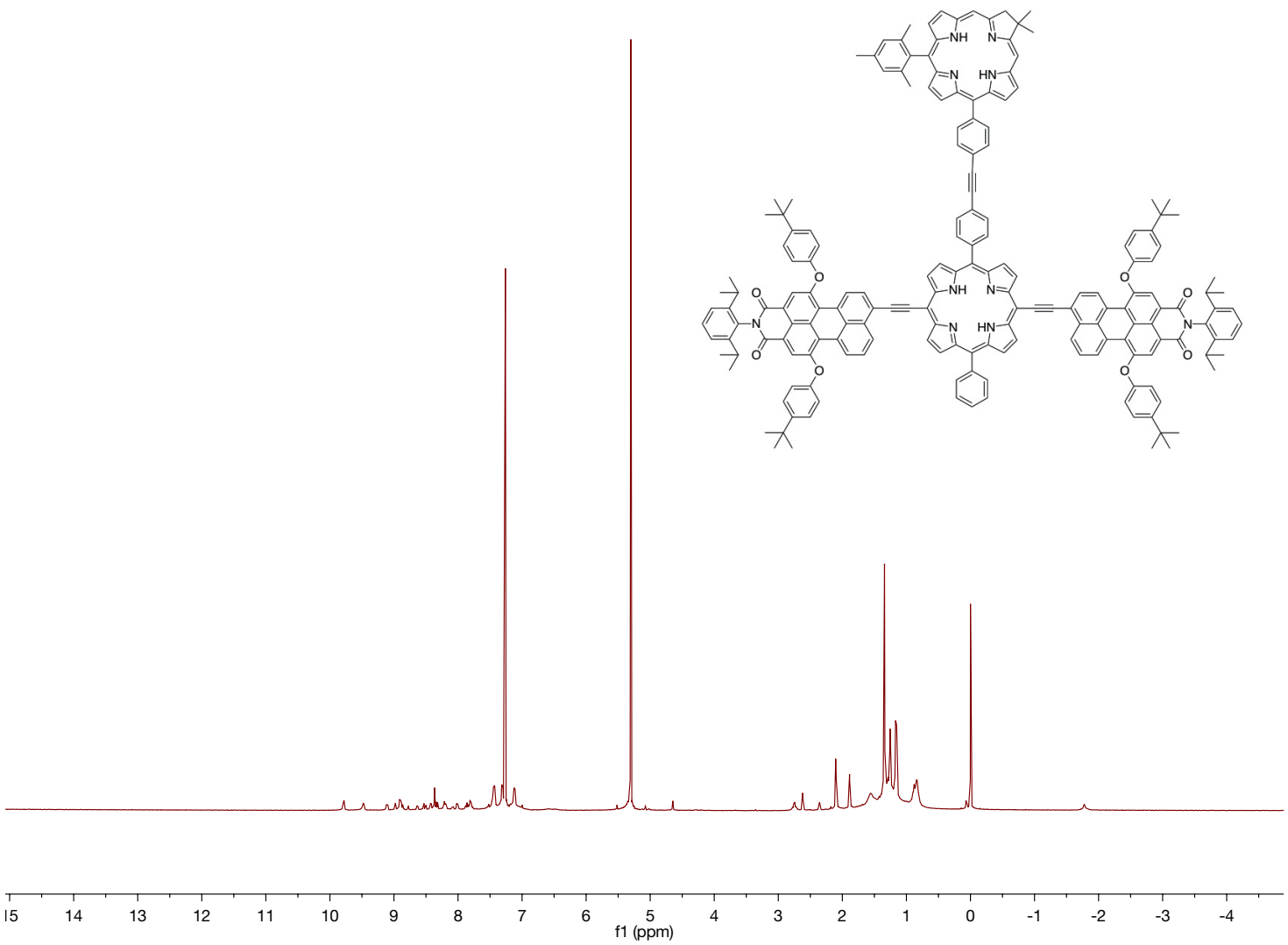

Figure S35. The ^{1}H NMR spectrum of **C-T**.

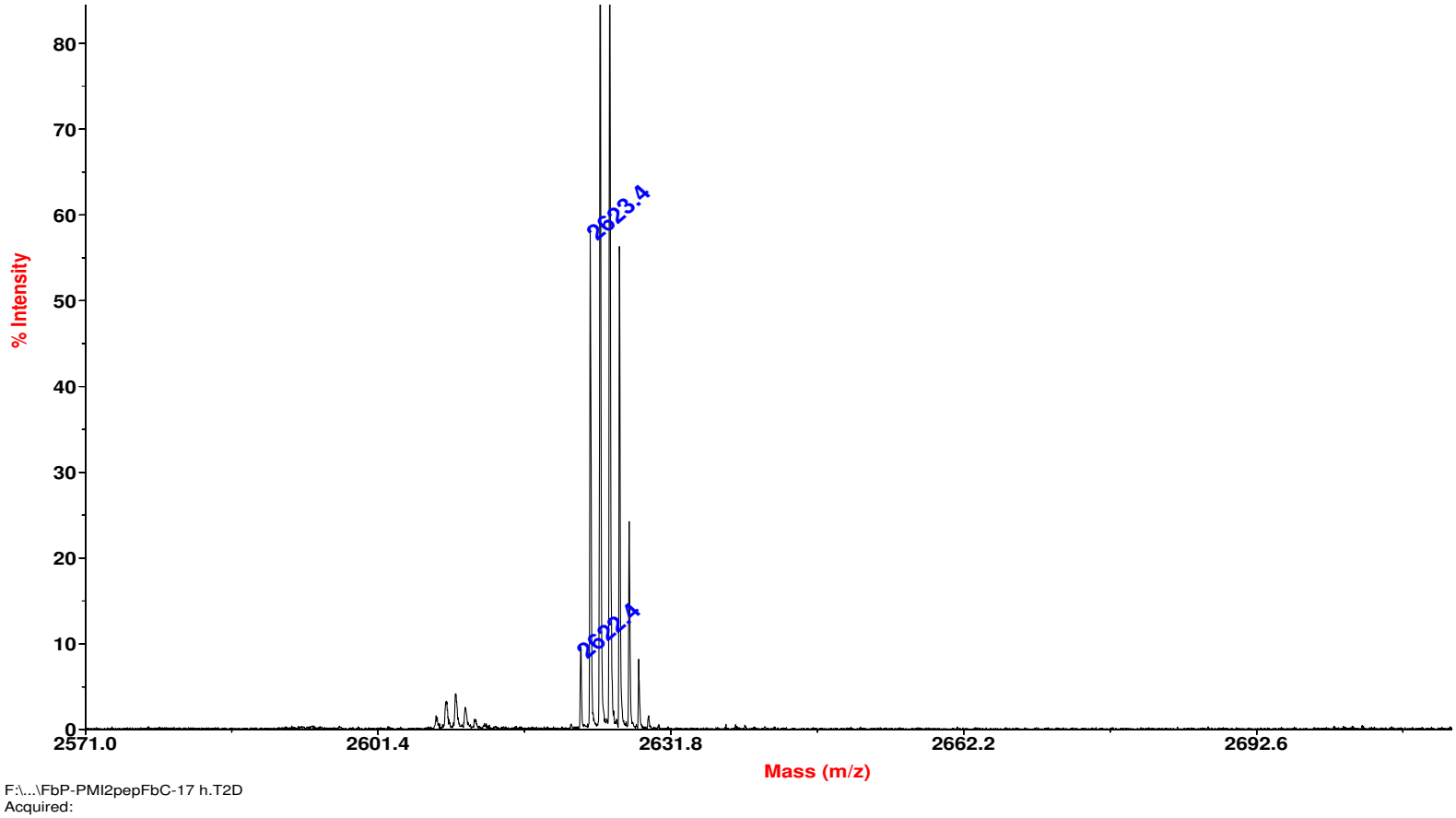

Figure S36. The MALDI-MS spectrum of **C-T**.

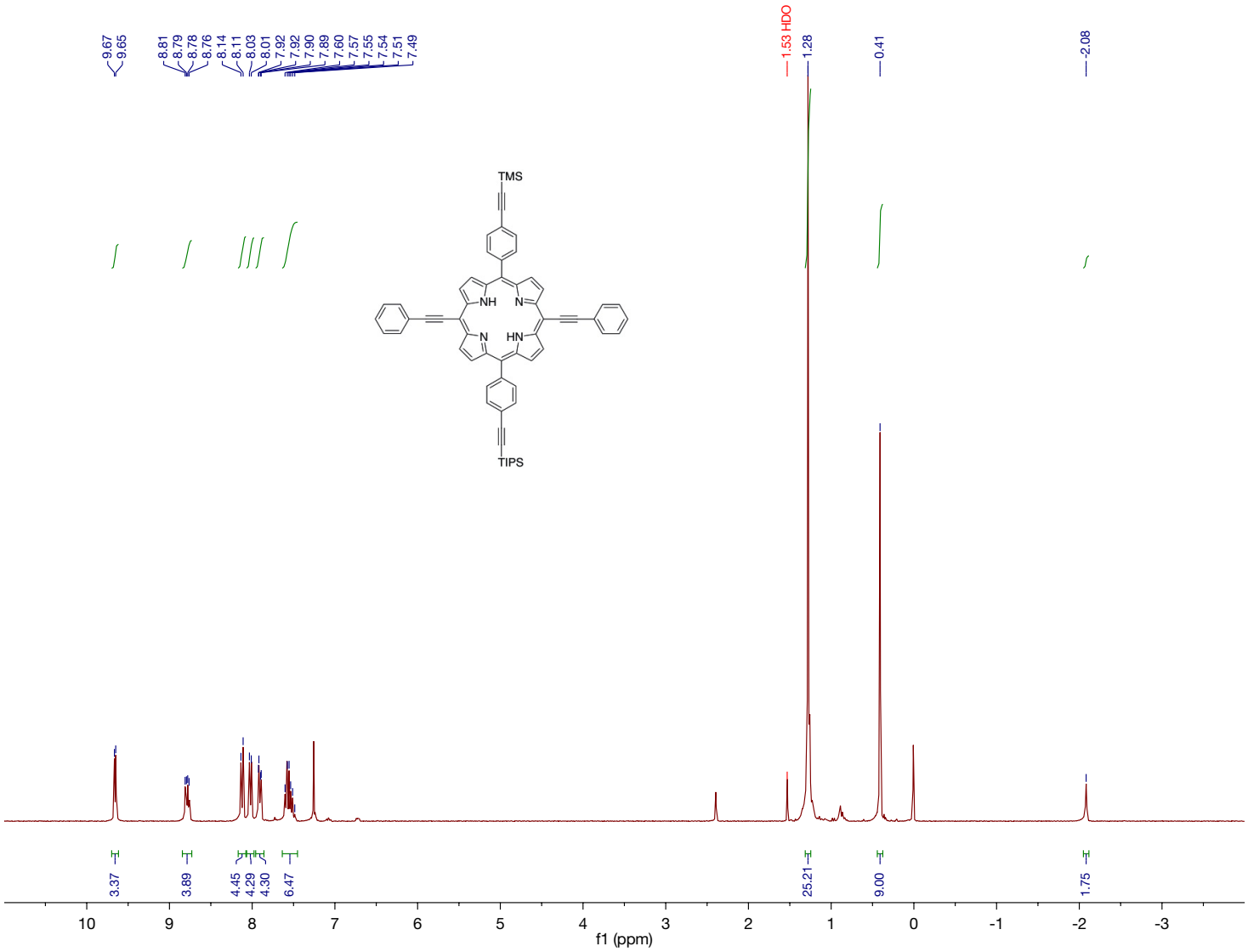

Figure S37. The ^{1}H NMR spectrum of **P-TMS/TIPS**.

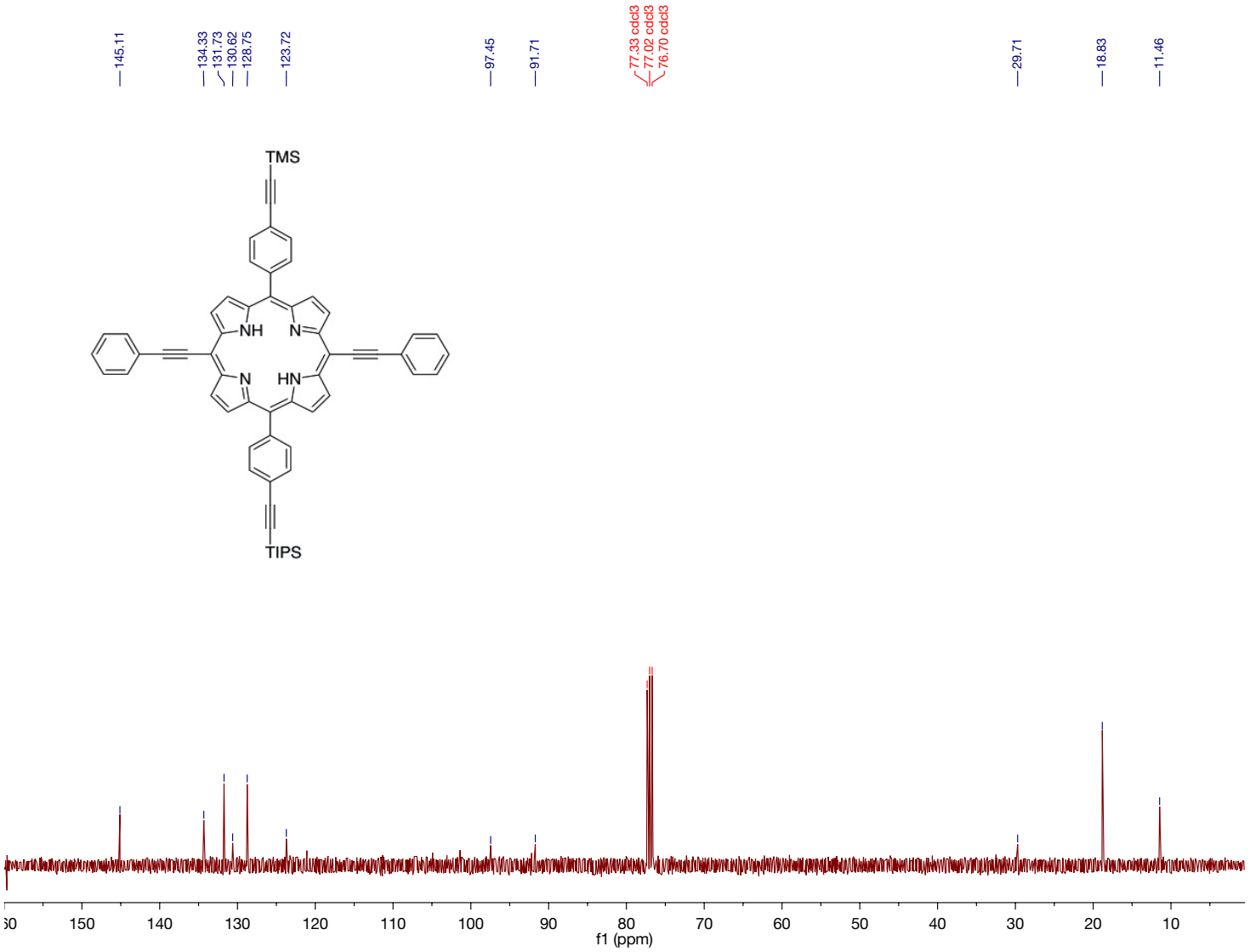

Figure S38. The ^{13}C NMR spectrum of **P-TMS/TIPS**.

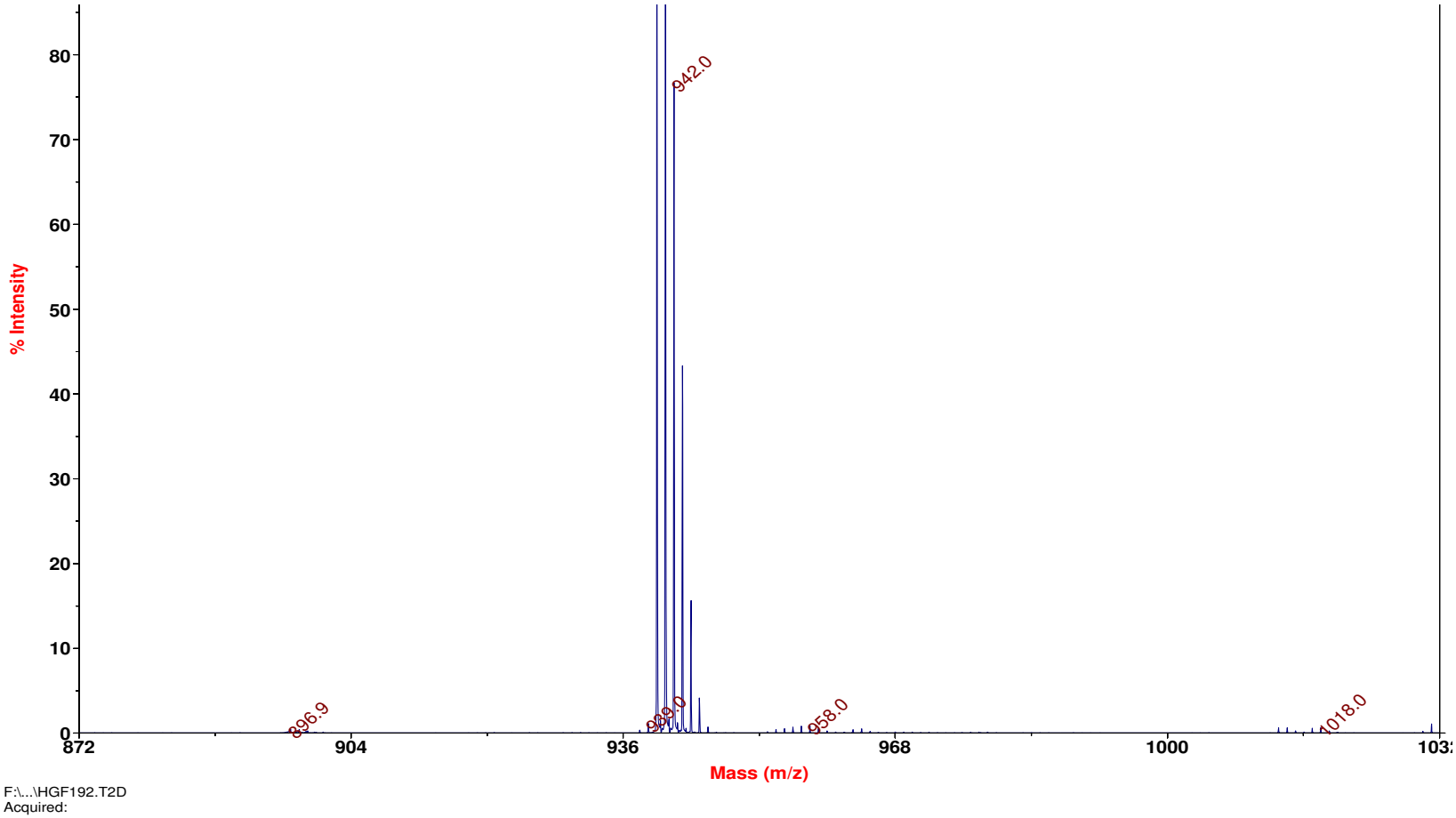

Figure S39. The MALDI-MS spectrum of **P-TMS/TIPS**.

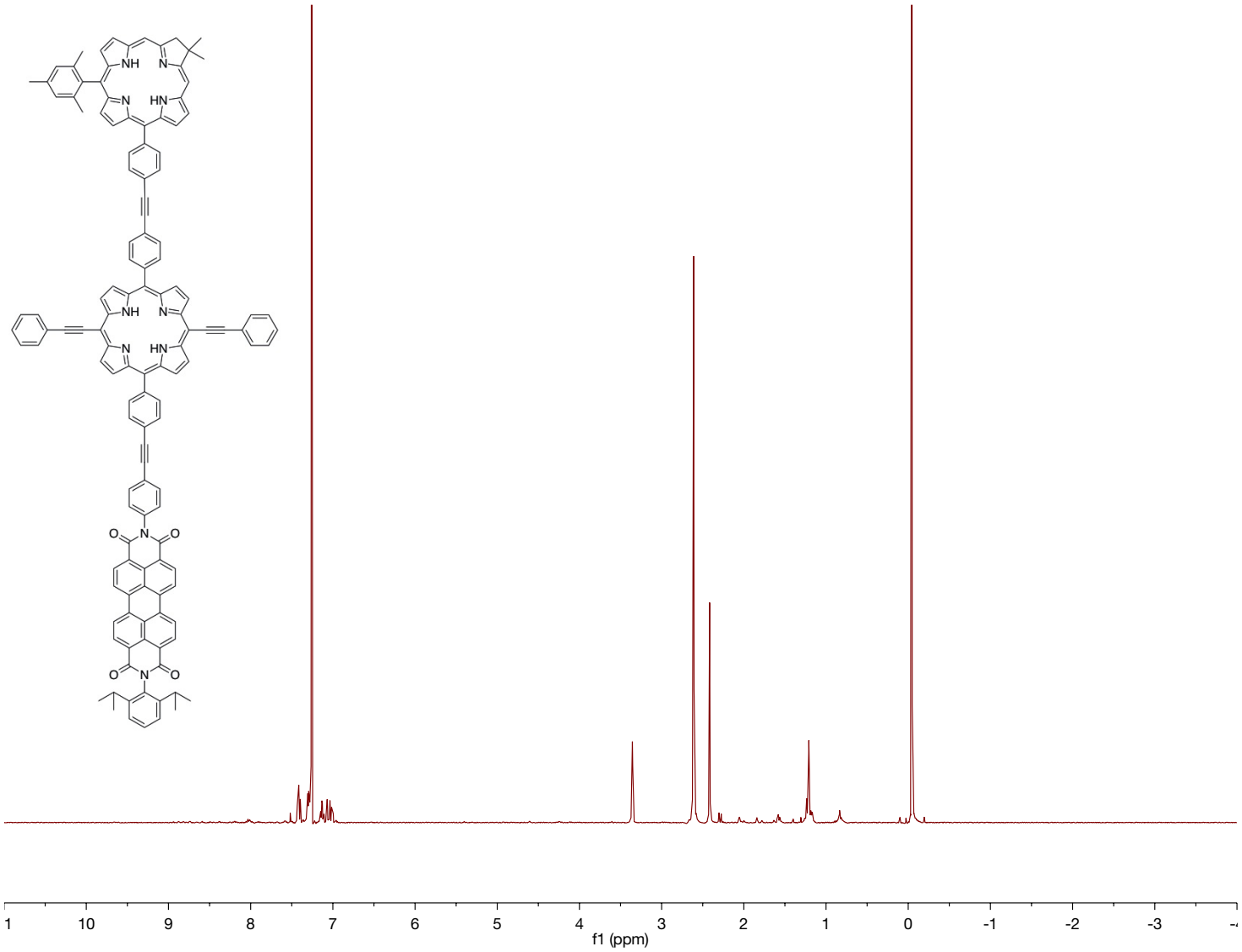

Figure S40. The ^{1}H NMR spectrum of **C-P-PDI**.

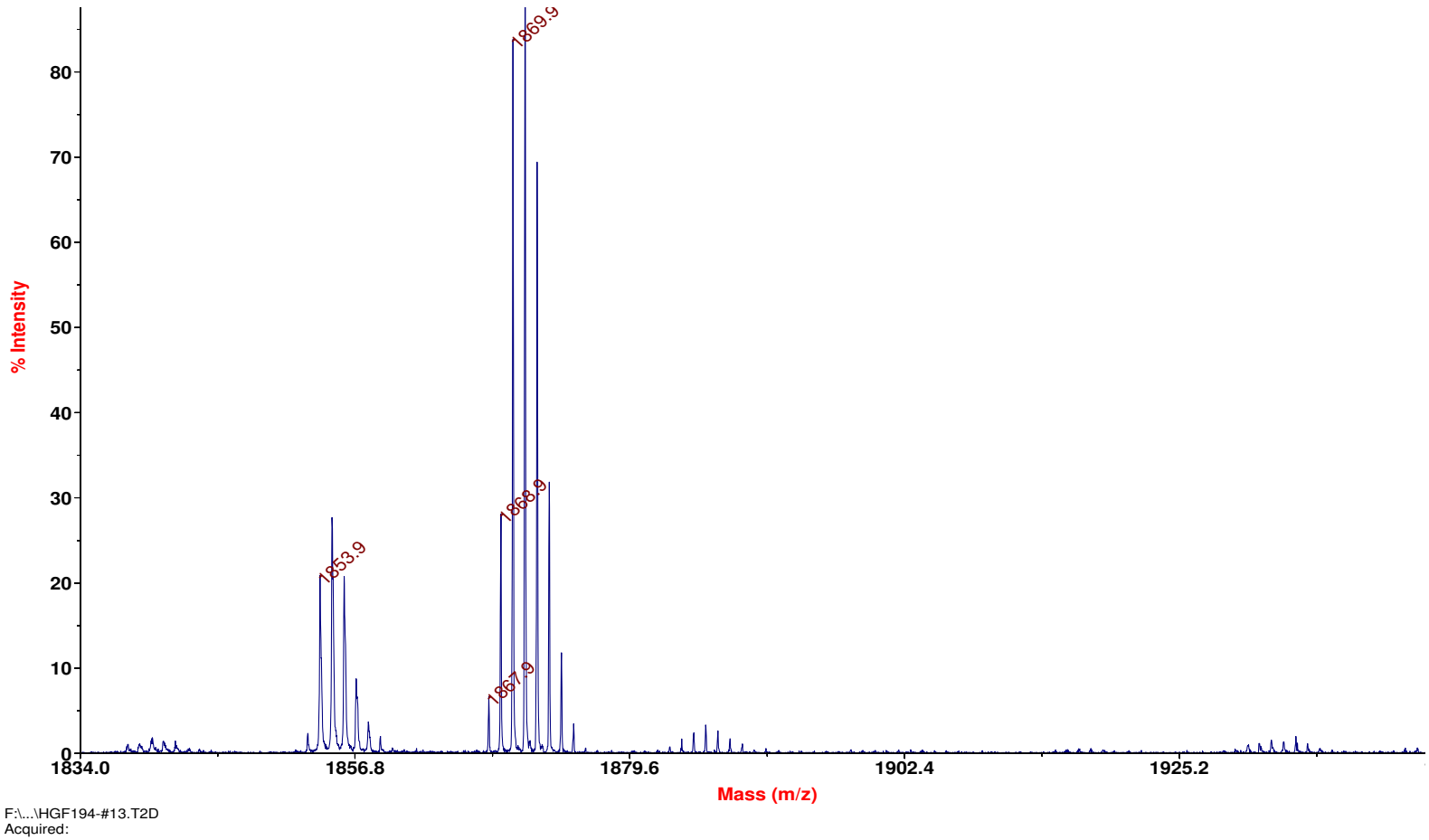

Figure S41. The MALDI-MS spectrum of **C-P-PDI**.

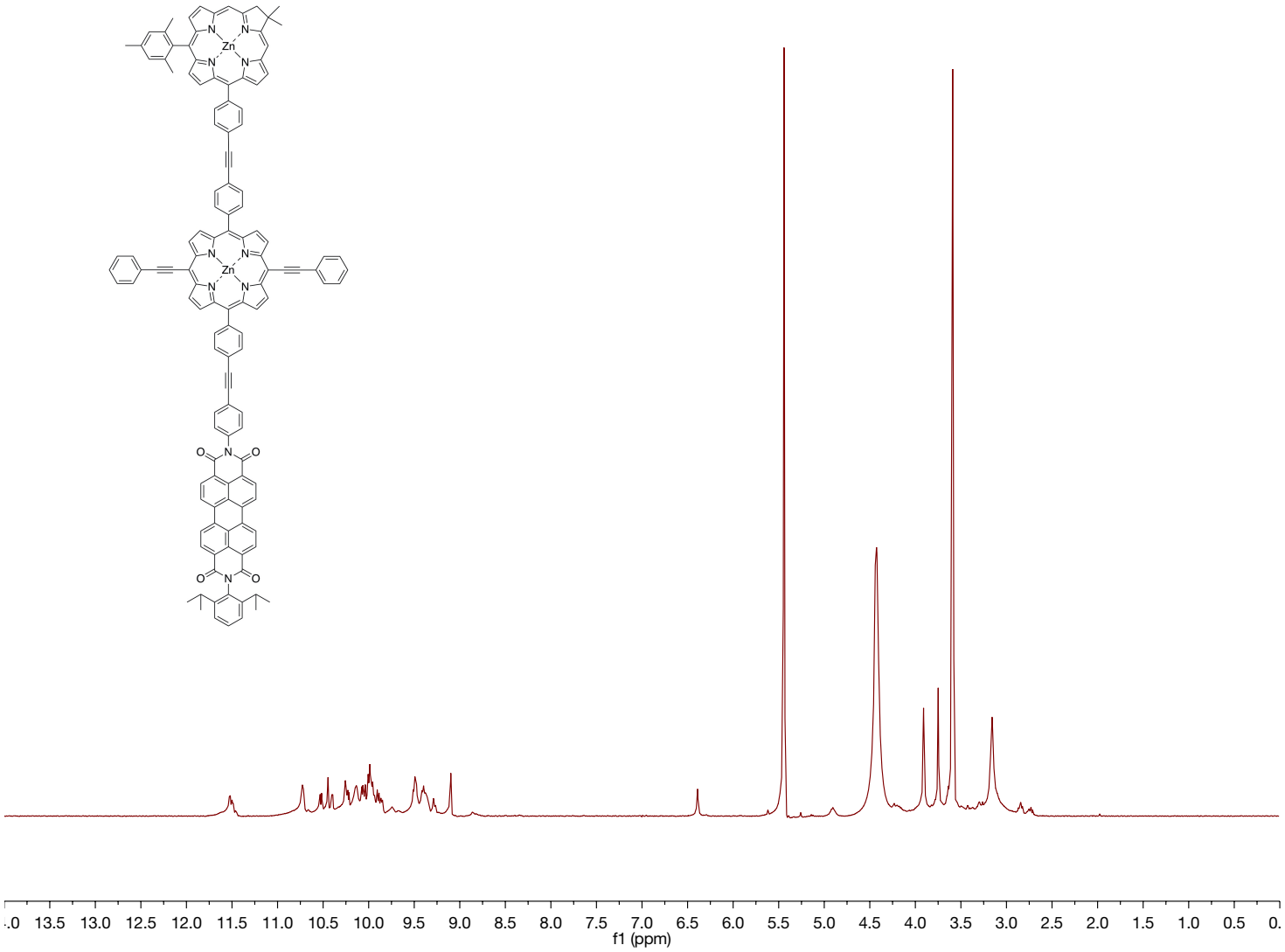

Figure S42. The ^{1}H NMR spectrum of **ZnC-ZnP-PDI**.

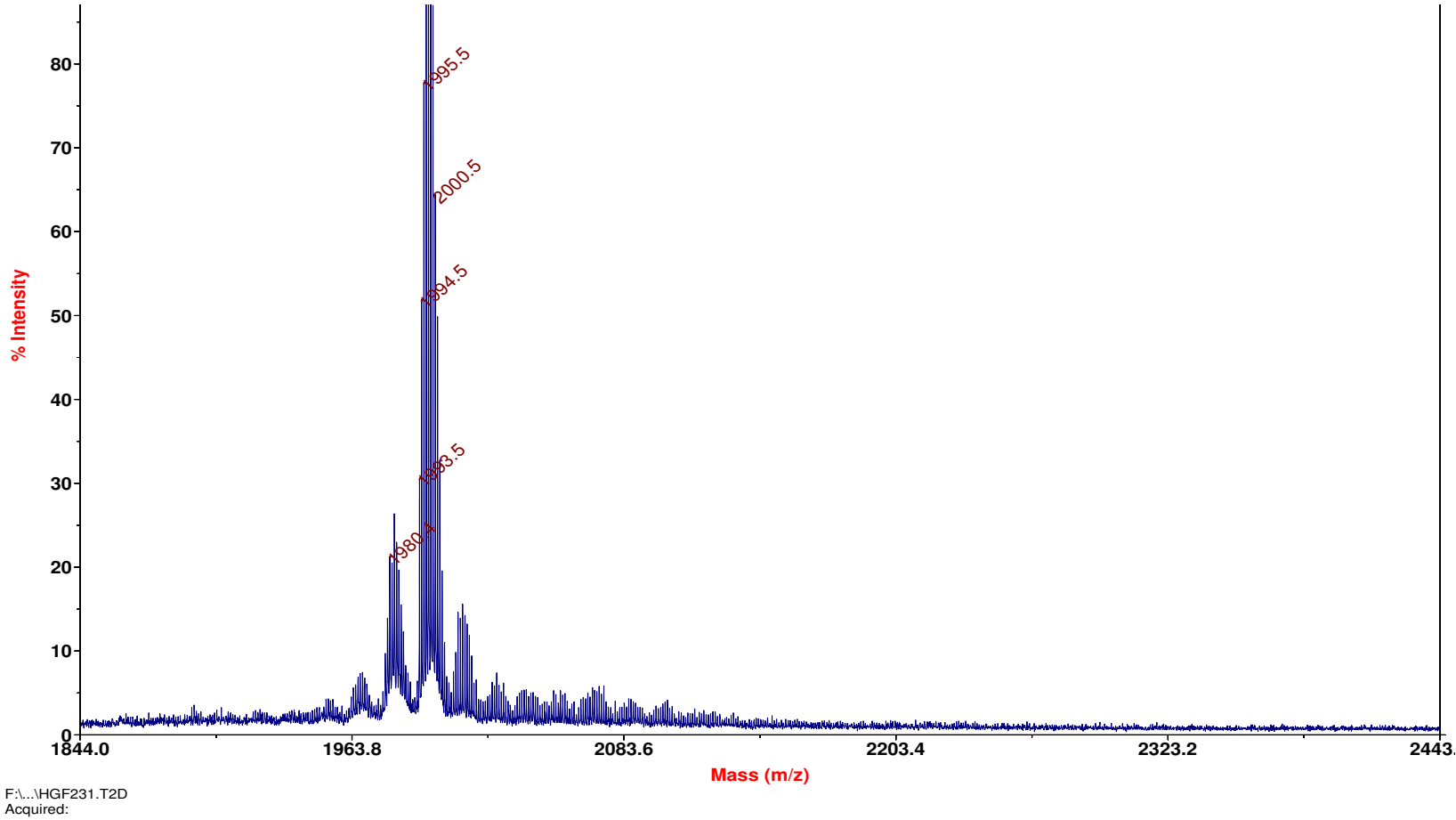

Figure S43. The MALDI-MS spectrum of **ZnC-ZnP-PDI**.

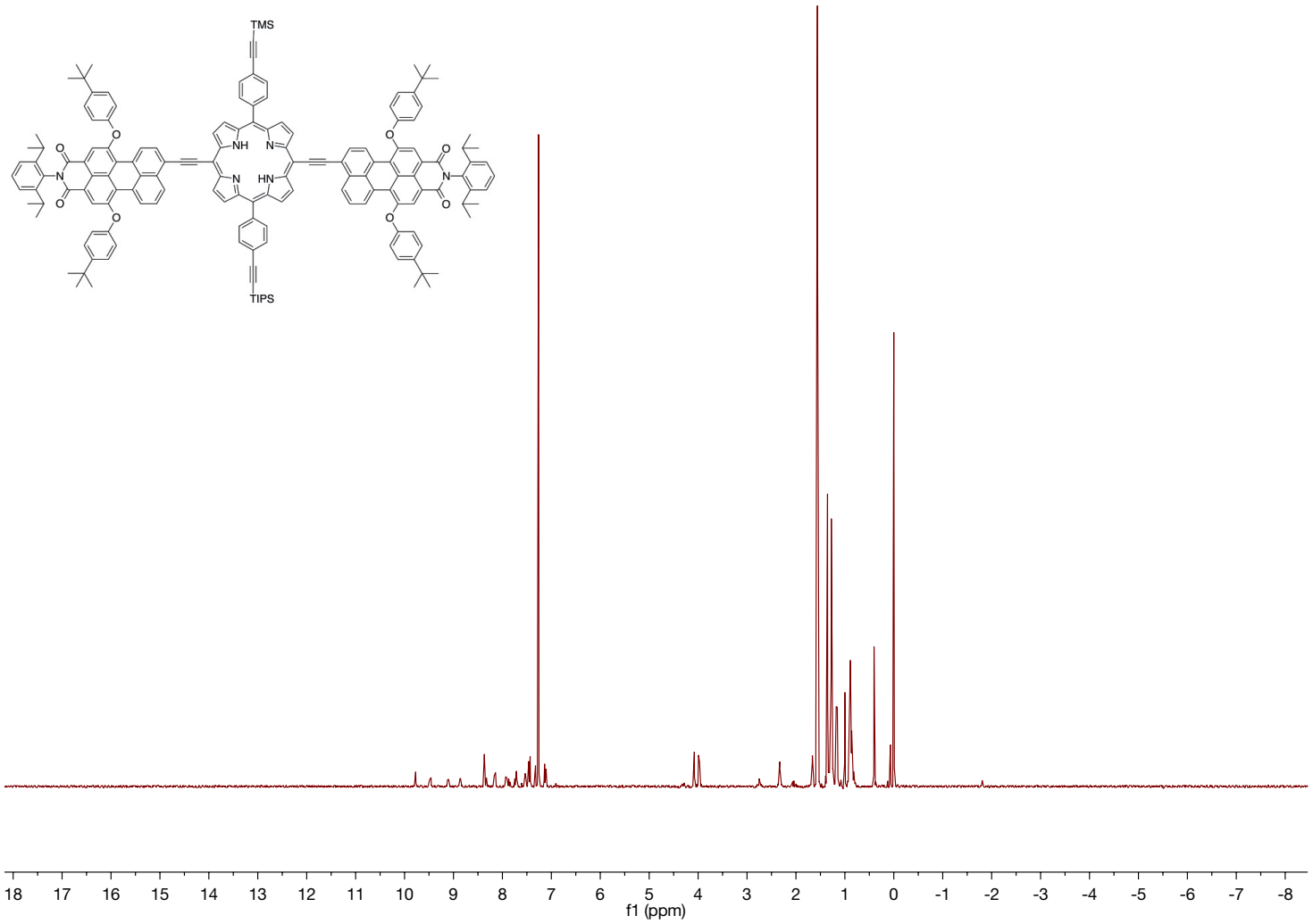

Figure S44. The ^{1}H NMR spectrum of **T-TMS/TIPS**.

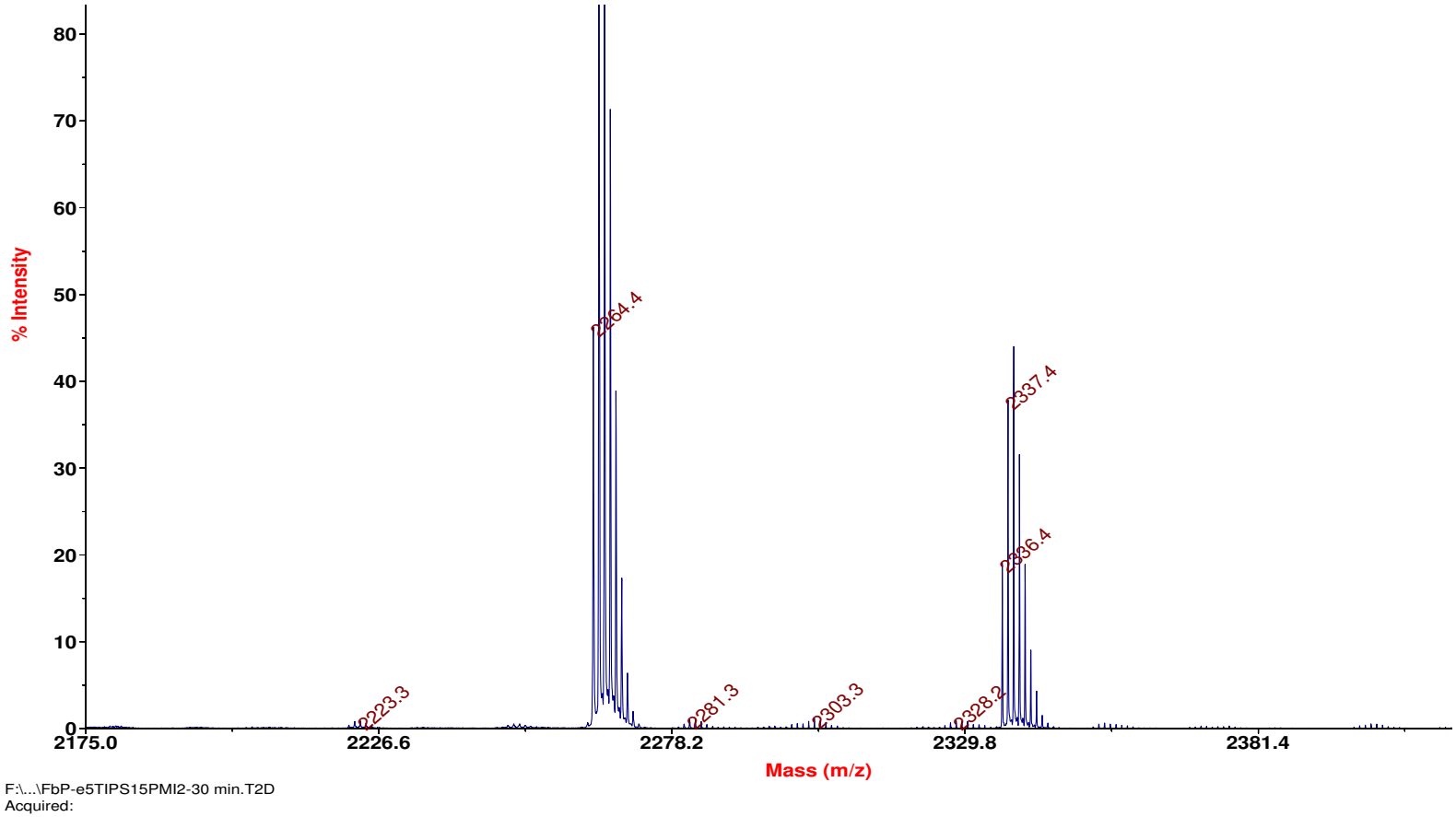

Figure S45. The MALDI-MS spectrum of **T-TMS/TIPS**.

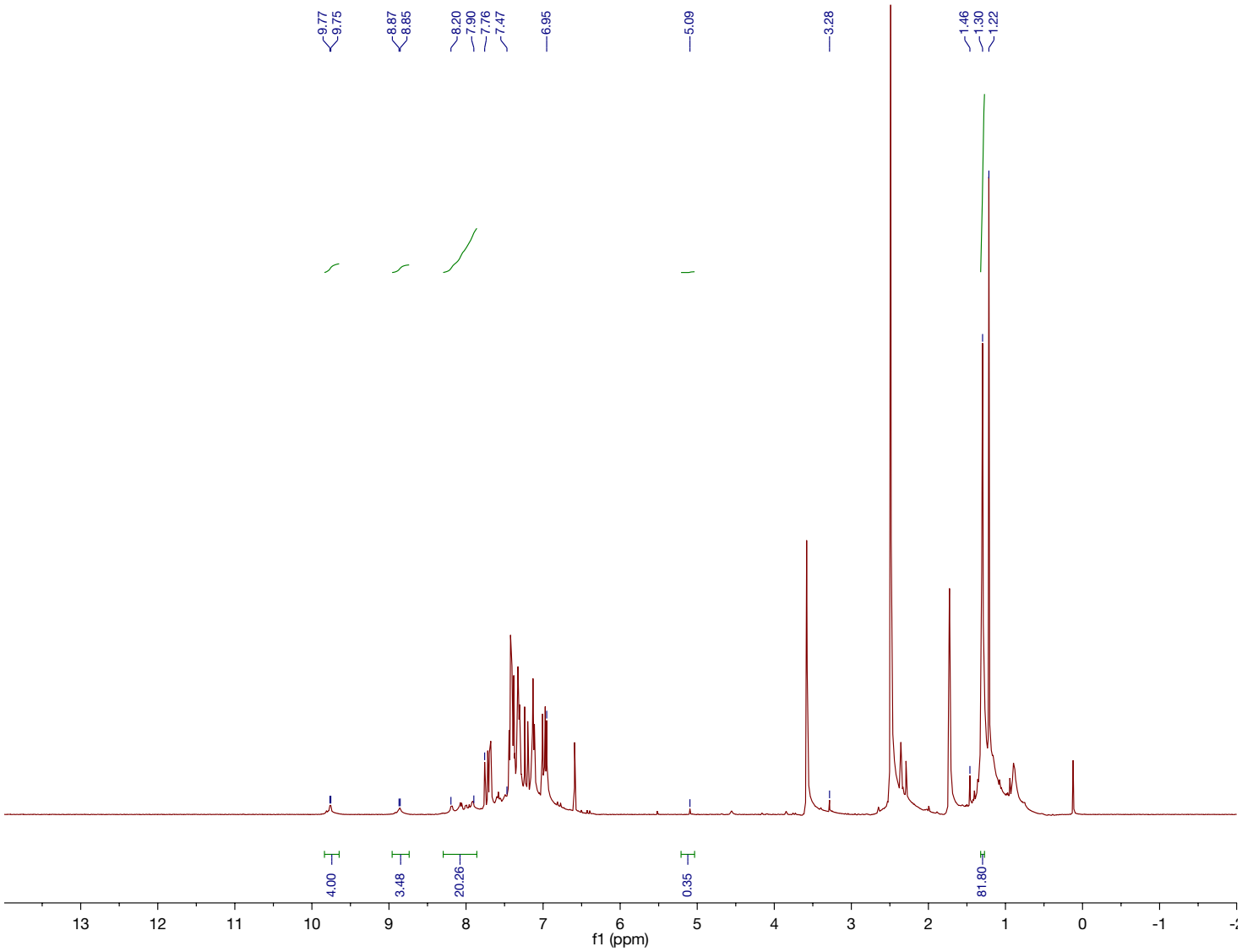

Figure S46. The ^{1}H NMR spectrum of **ZnP-H/TIPS**.

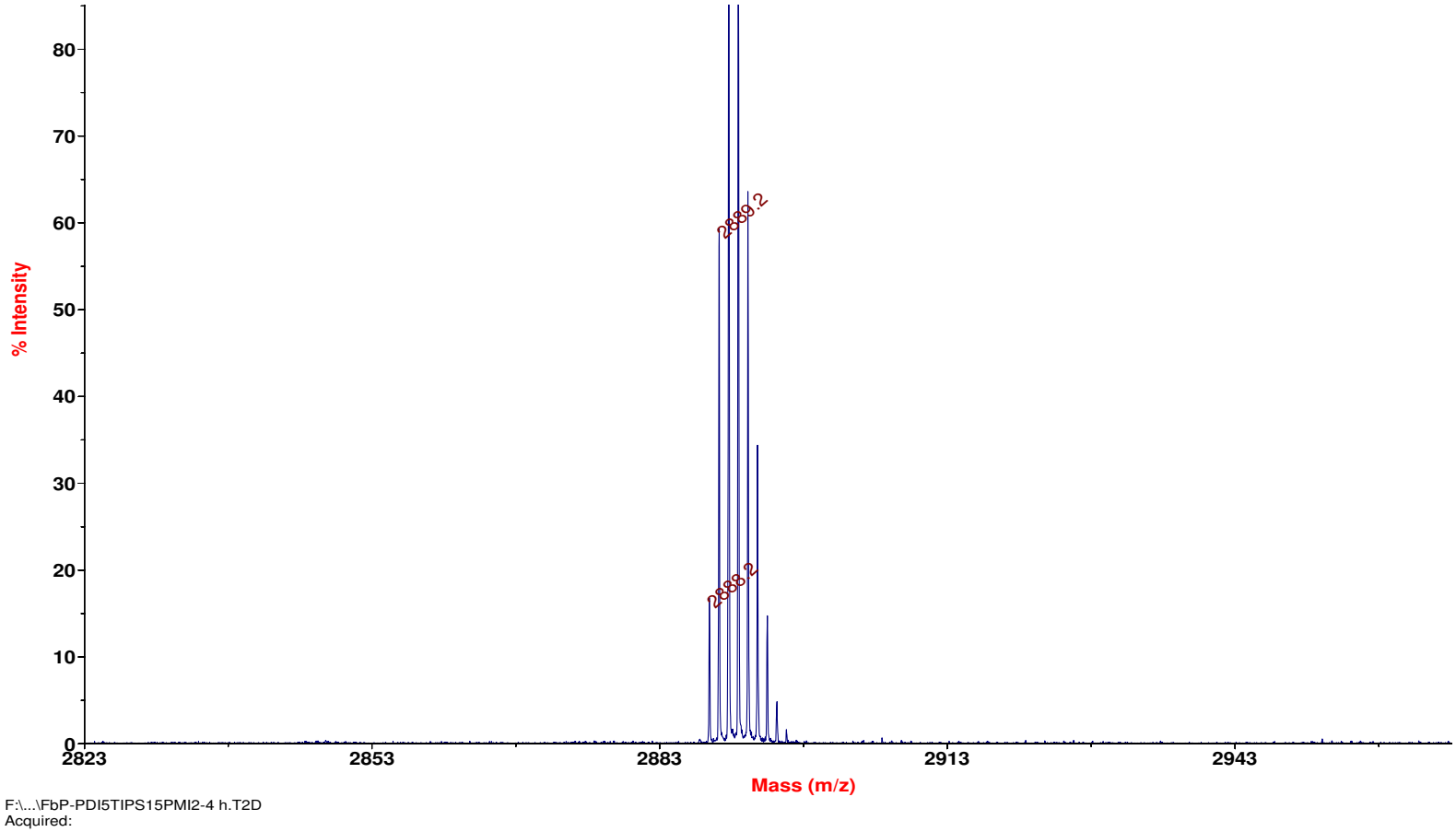

Figure S47. The MALDI-MS spectrum of **T-H/PDI**.

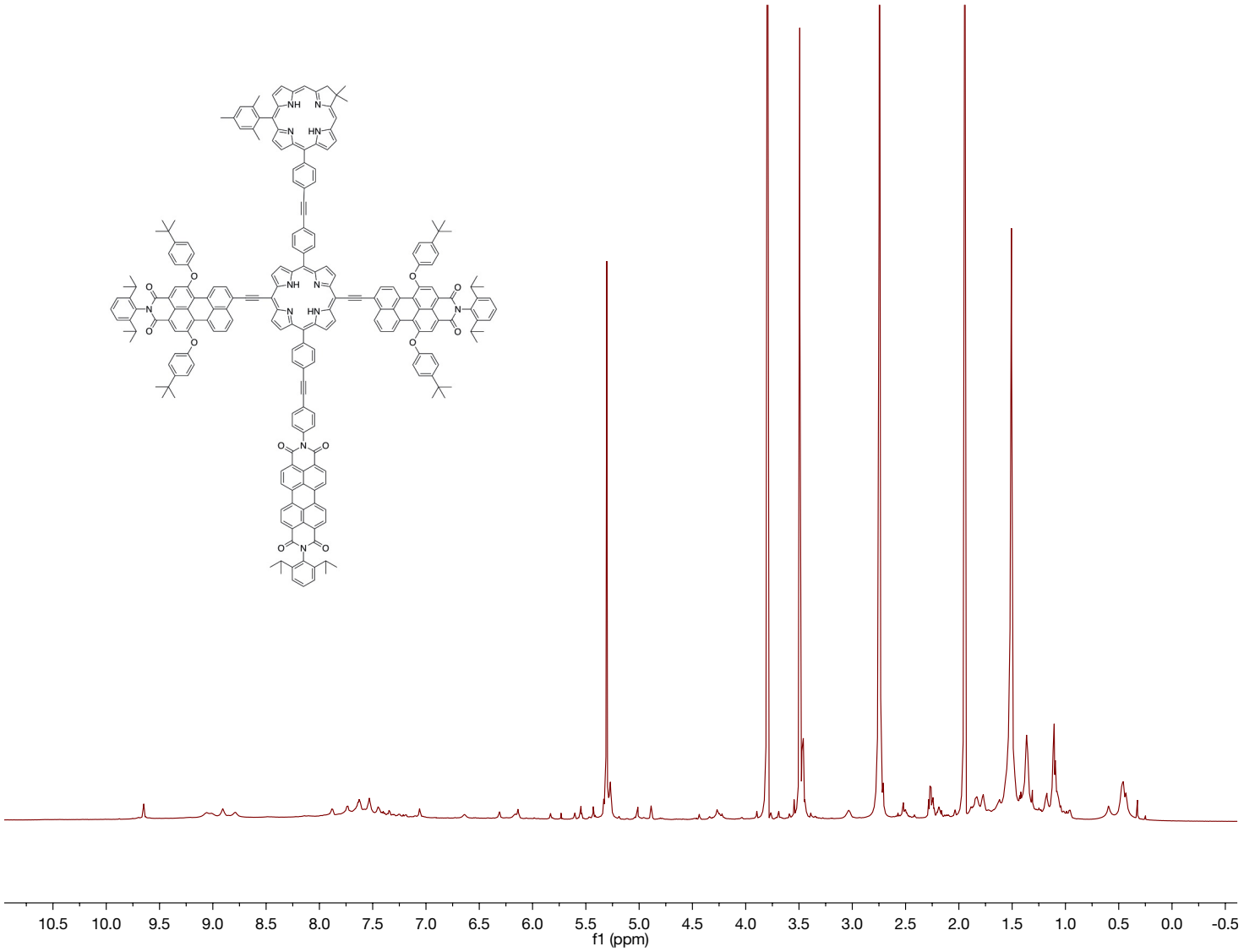

Figure S48. The ^{1}H NMR spectrum of **C-T-PDI**.

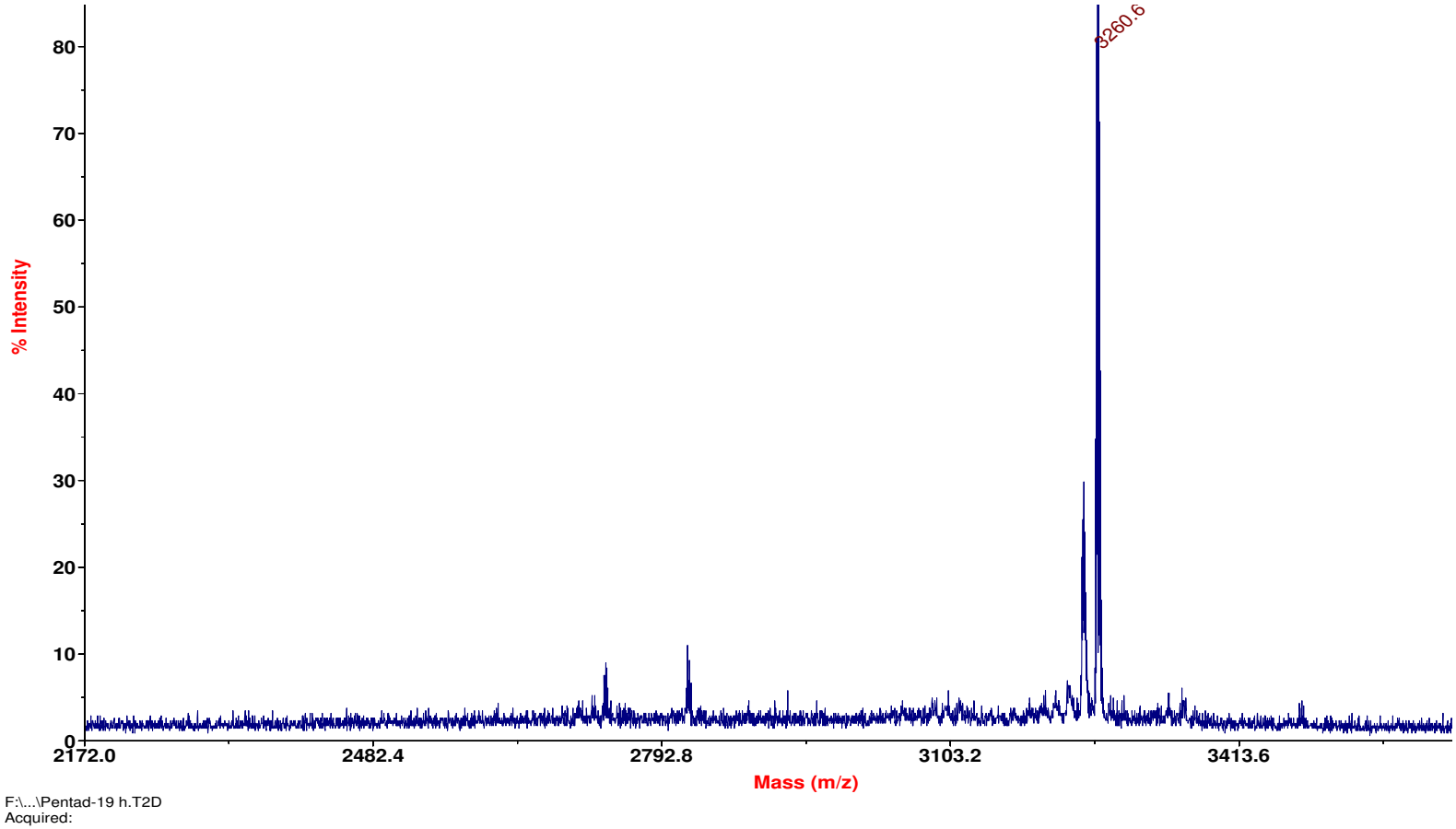

Figure S49. The MALDI-MS spectrum of **C-T-PDI**.

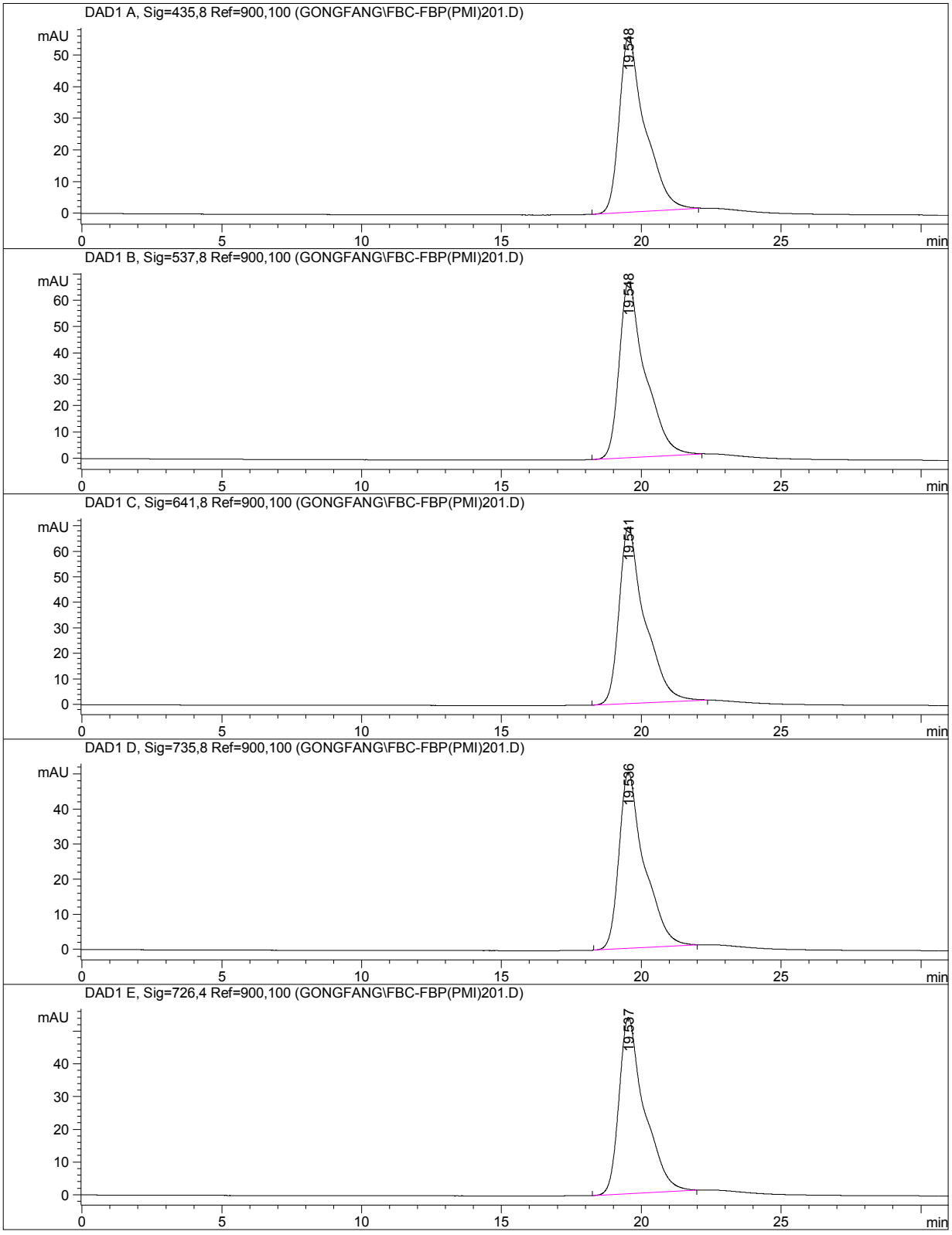

Figure S50. The HPLC trace of **C-T**.

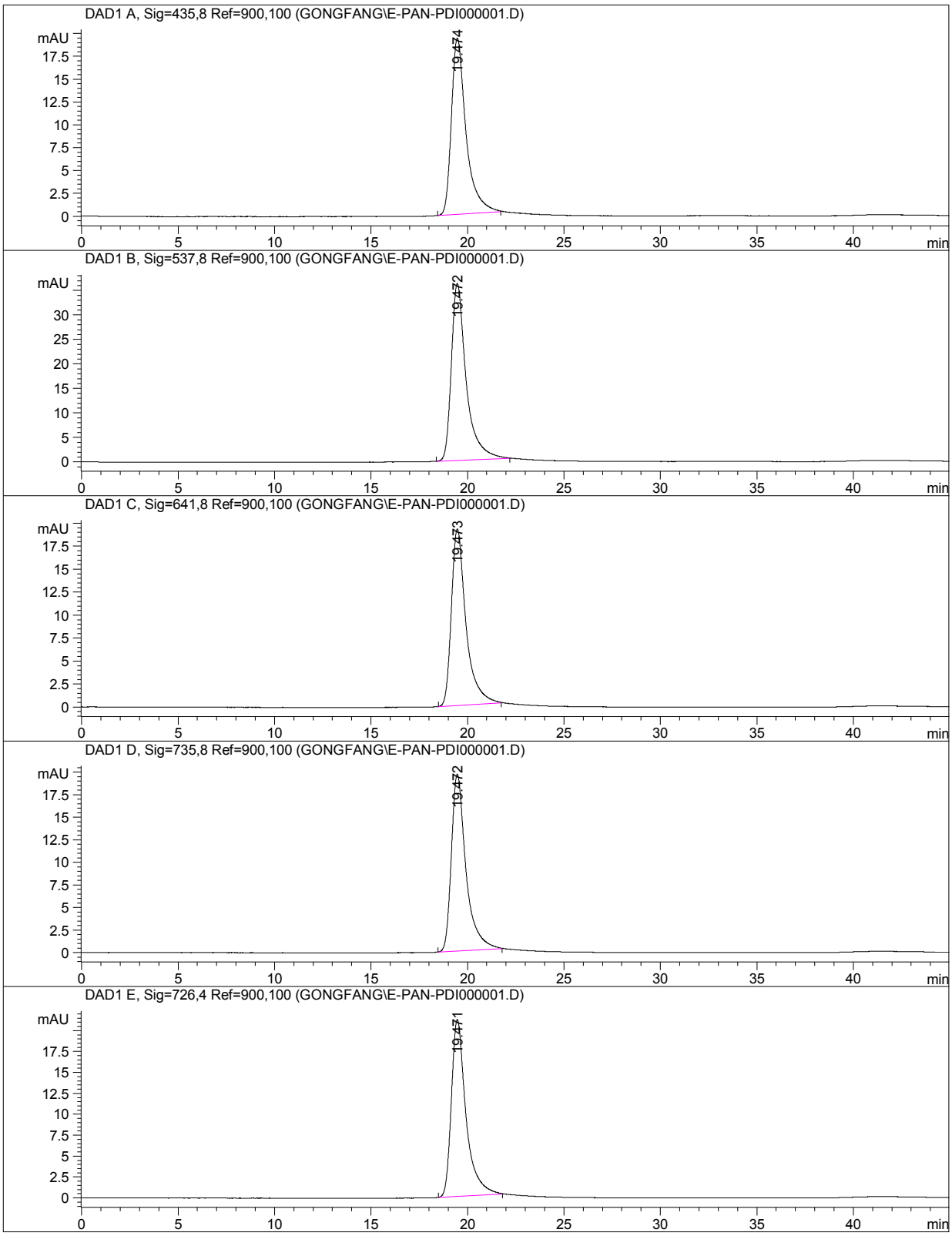

Figure S51. The HPLC trace of **T-H/PDI**

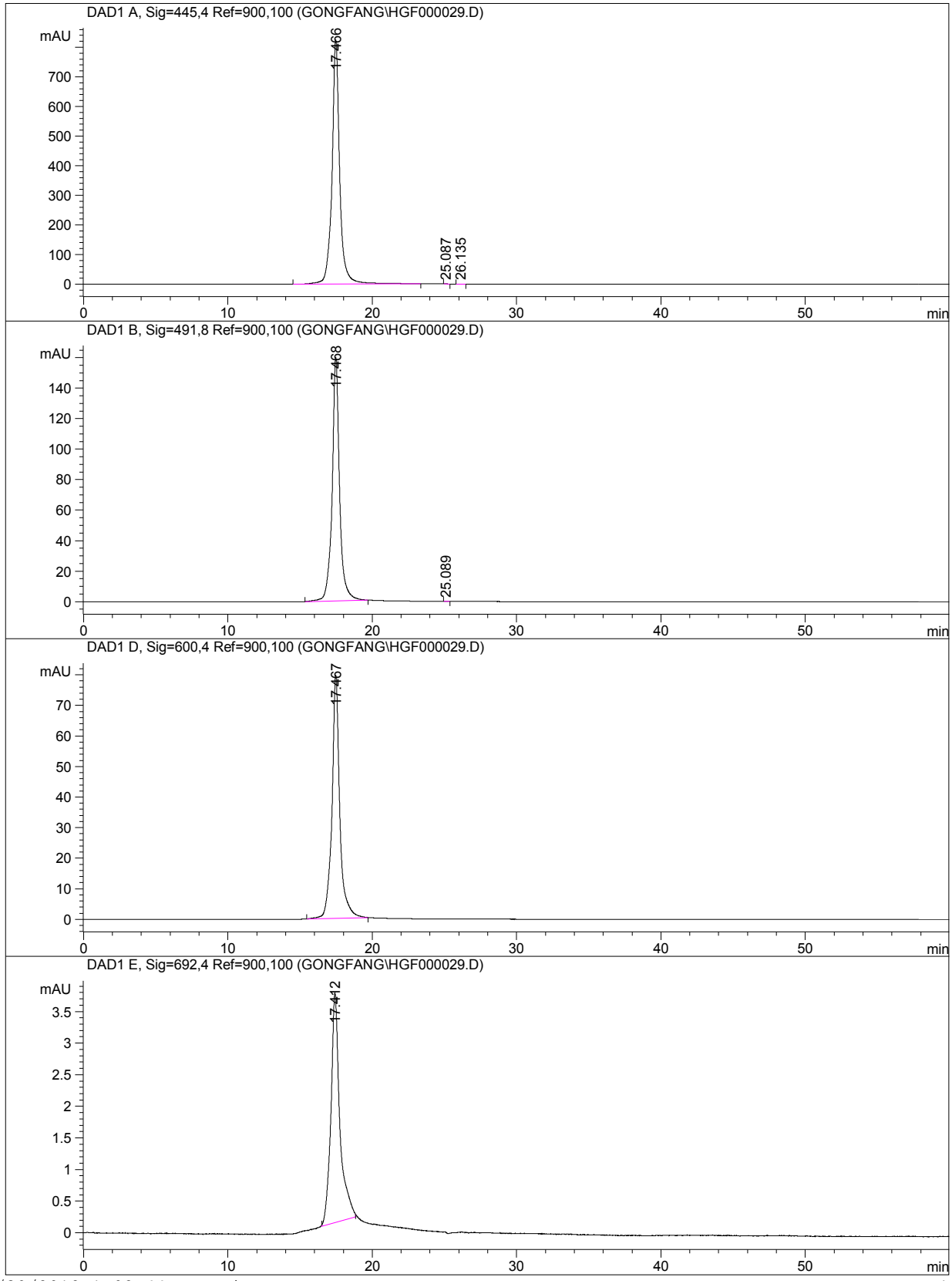

Figure S52. The HPLC trace of **ZnC-ZnP-PDI**.

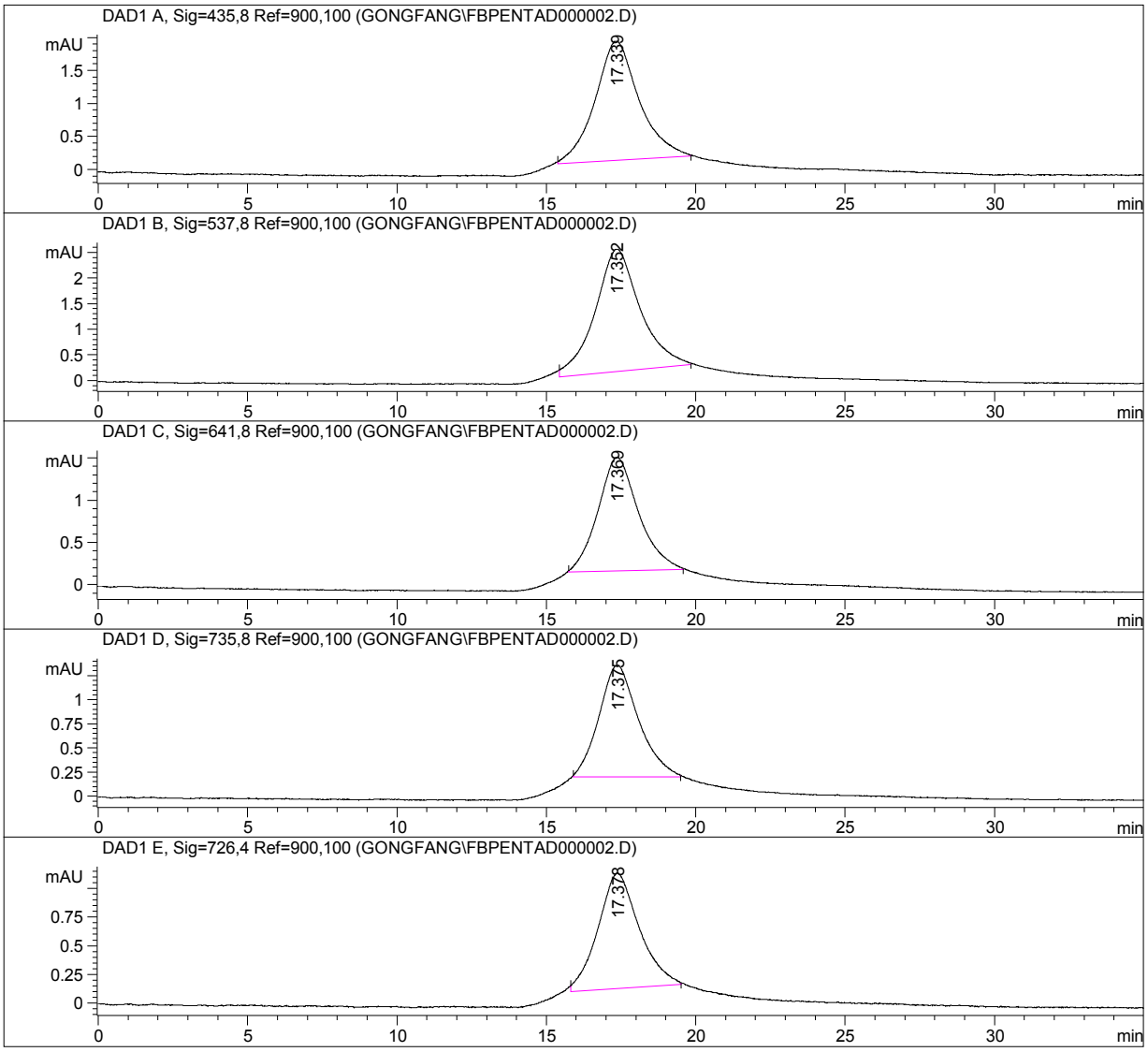

Figure S53. The HPLC trace of **C-T-PDI**.

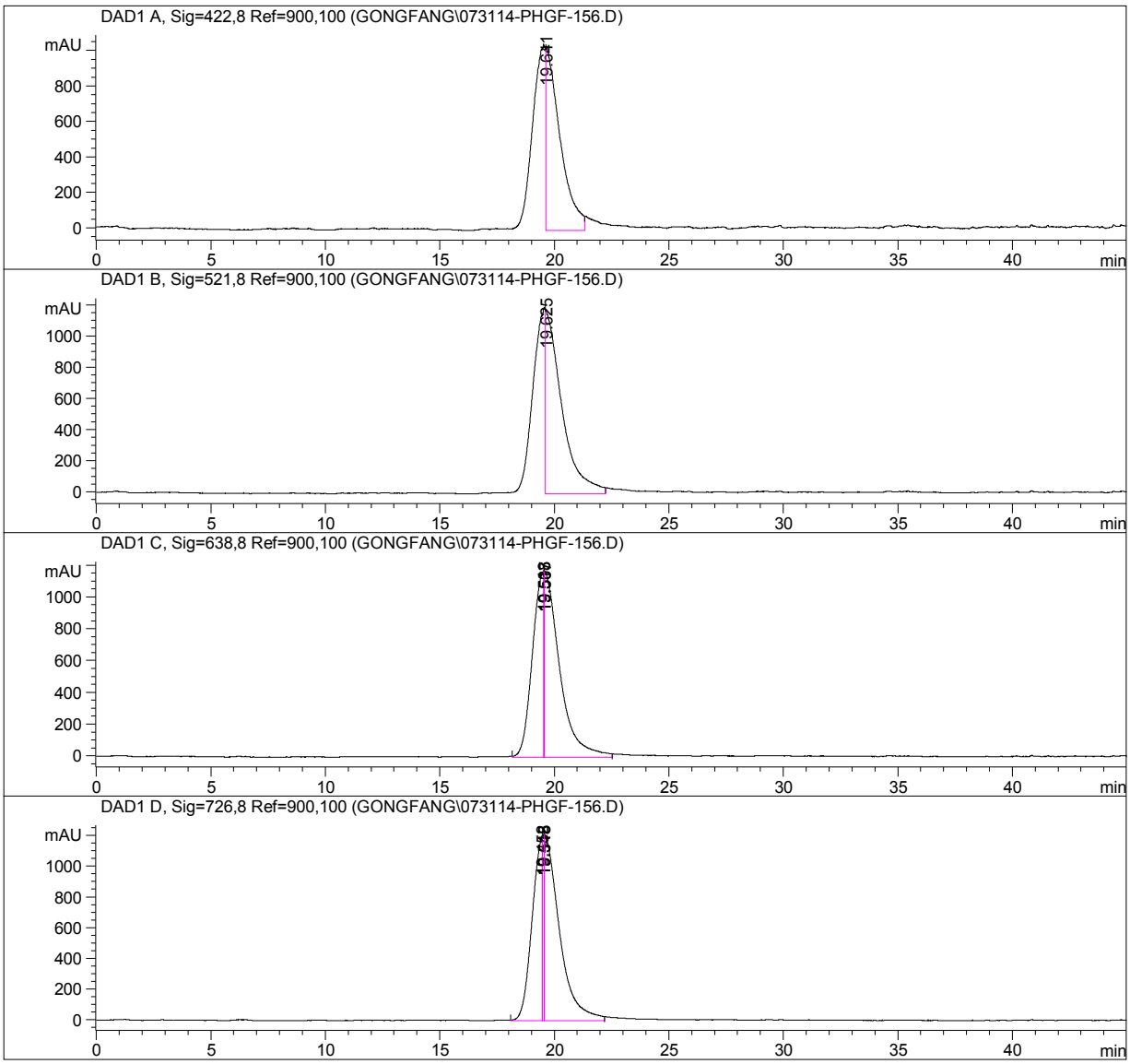

Figure S54. The HPLC trace of **T-Ph**.

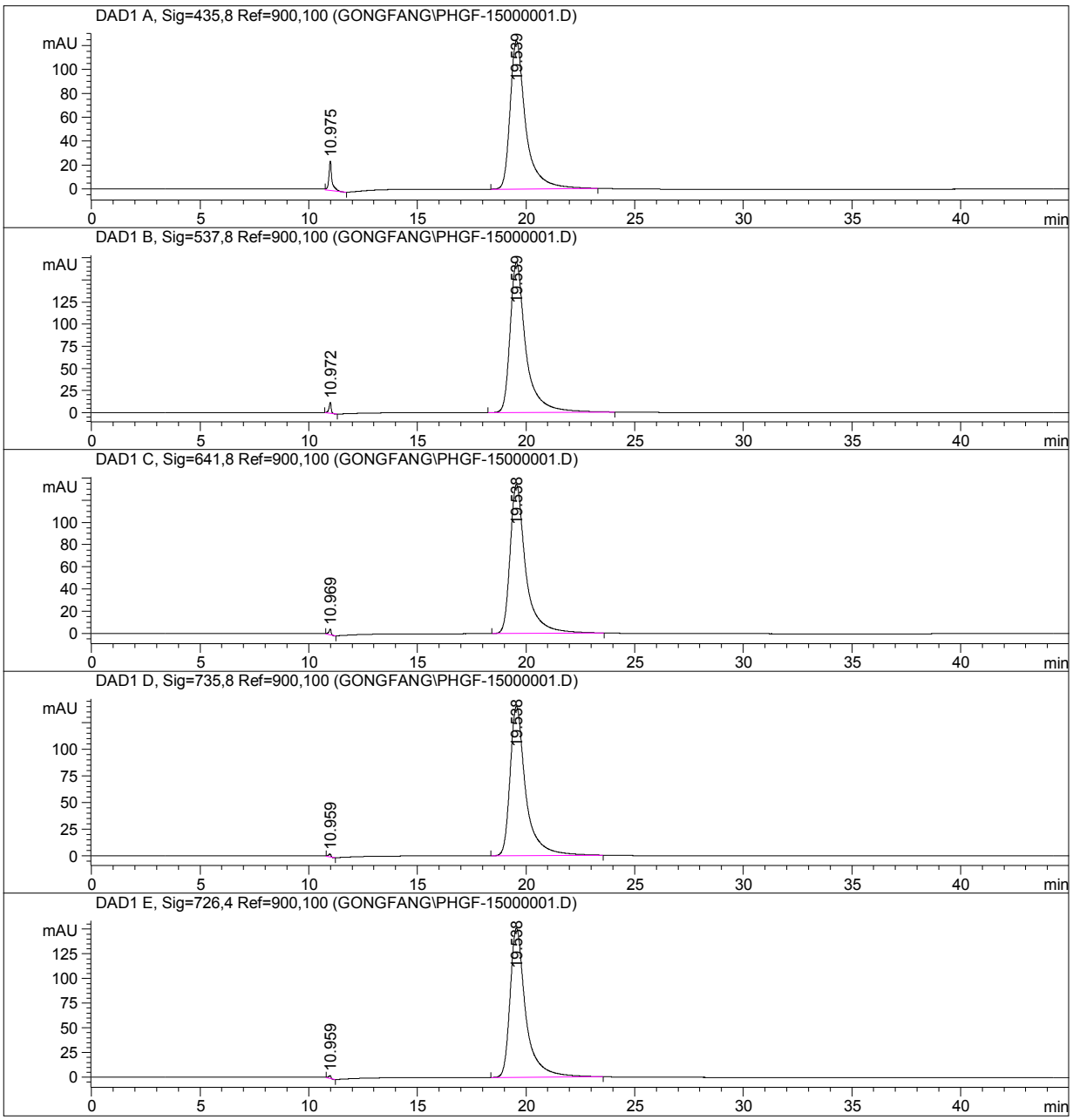

Figure S55. The HPLC trace of **T-Ph-H**.

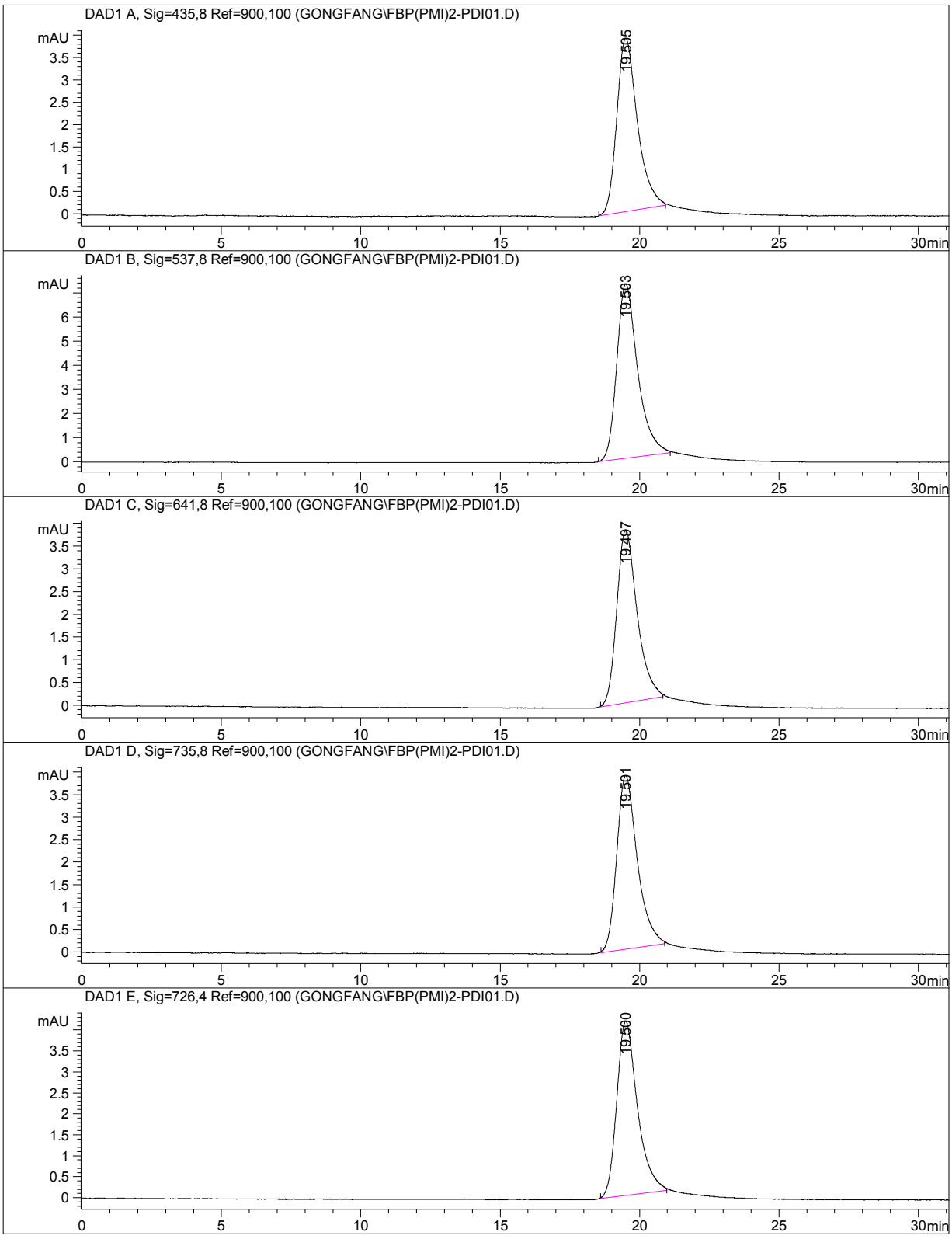

Figure S56. The HPLC trace of **T-PDI**.

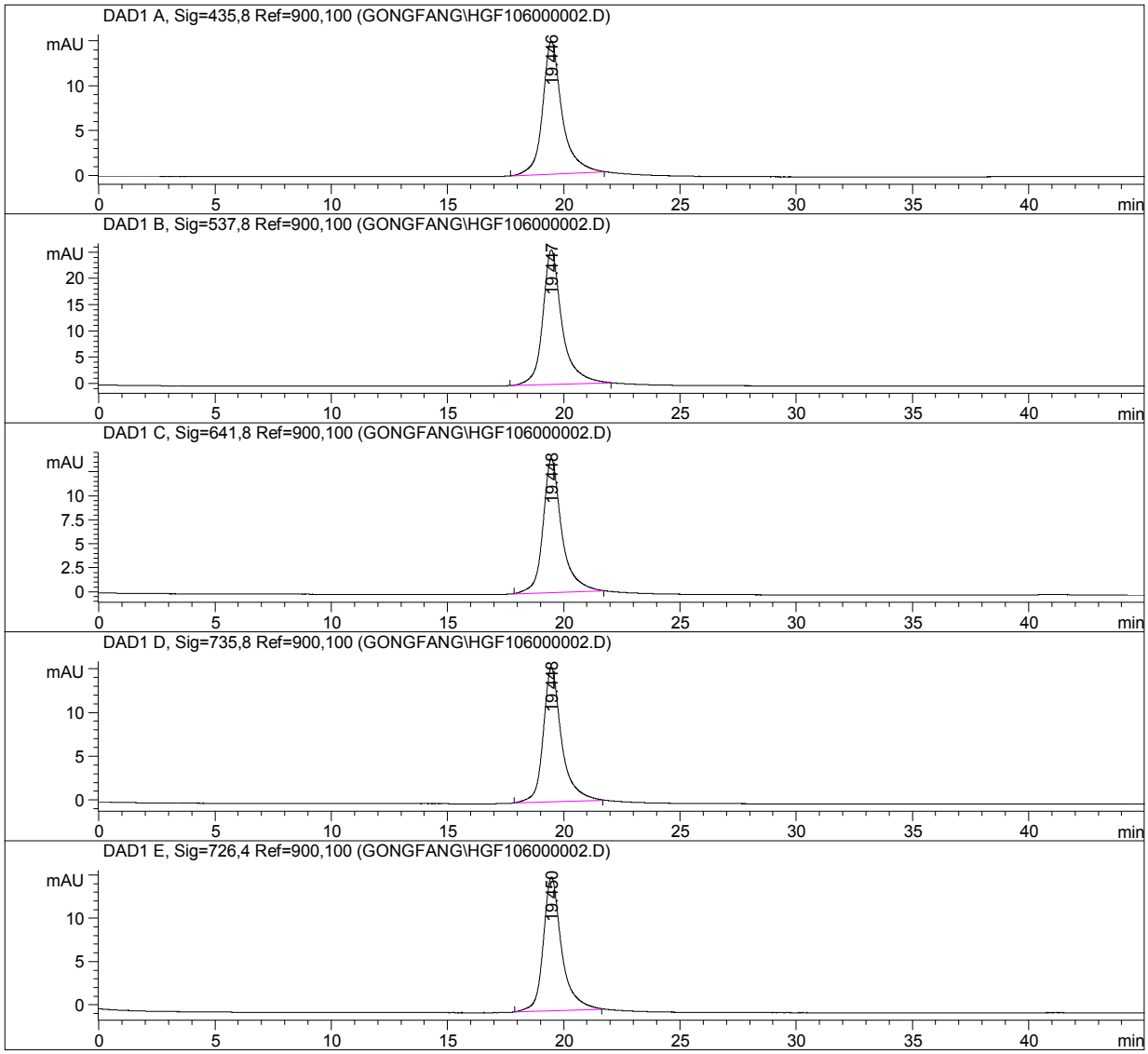

Figure S57. The HPLC trace of **T-TMS/TIPS**.

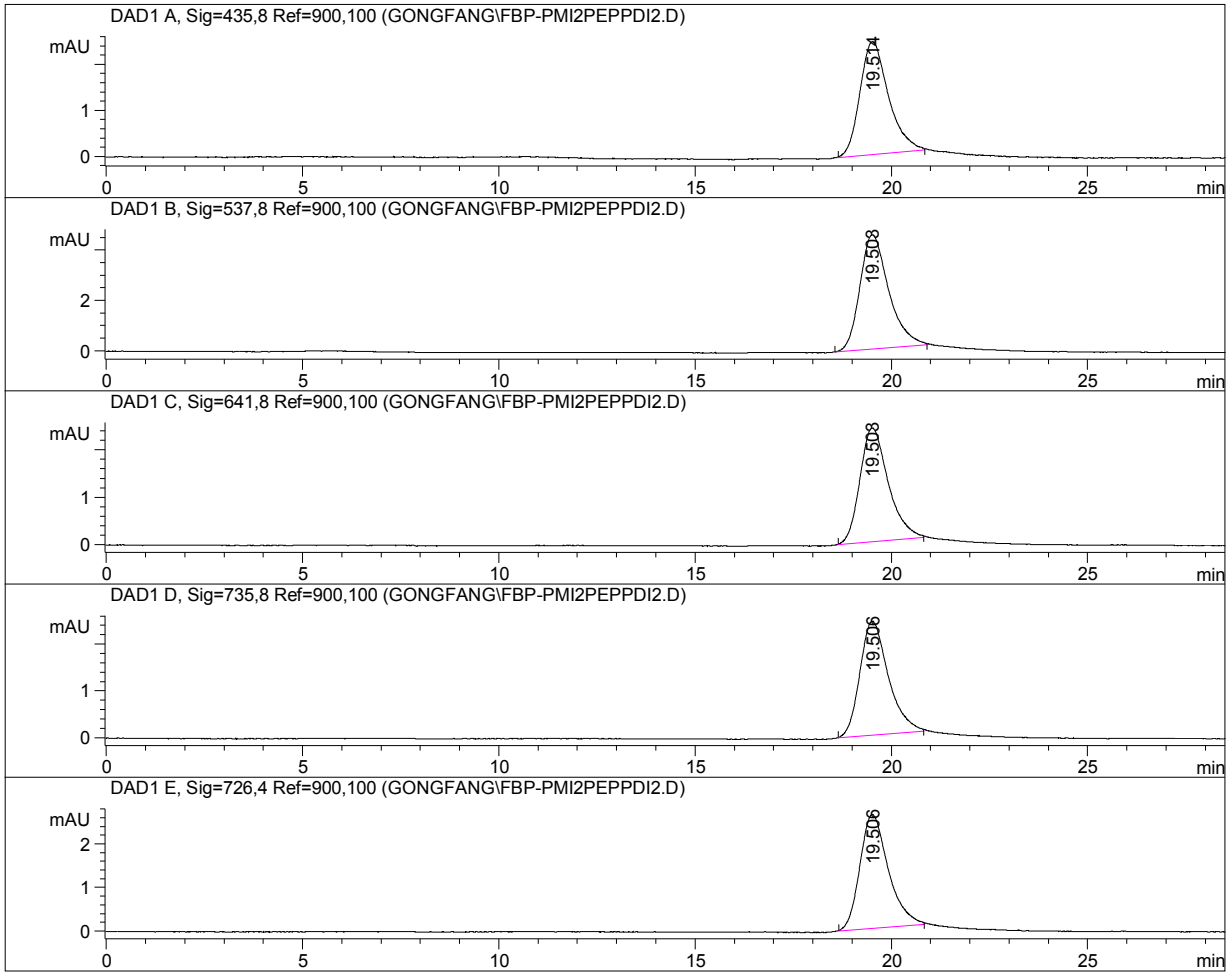

Figure S58. The HPLC trace of **ZnT-PDI**.

Analytical SEC monitoring of the formation of pentad C-T-PDI.

The Sonogashira coupling reaction of **T-H/PDI** and **5** was monitored with analytical size exclusion chromatography (SEC), as has been done previously with multiporphyrin arrays.[31,32] The precursor **T-H/PDI** was determined to be 99% pure according to the analytical SEC trace (Figure S59, panel A). After the one-hour reaction, an aliquot of the reaction mixture was analyzed to show four peaks (panel B). The dominant peak was assigned to the unreacted **T-H/PDI** based on the retention time and corroborative MALDI-MS data. The retention time of the purified form of the pentad (panel C) and corroborative MALDI-MS and absorption data revealed that the leading peak in panel B was the desired pentad product. The other two small peaks were presumed to be some tetrapyrrolic impurities.

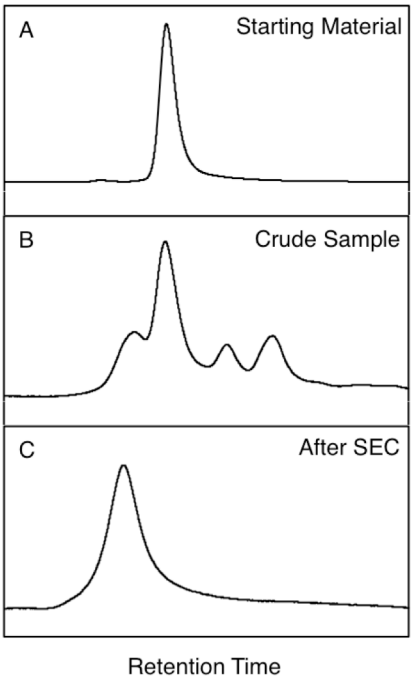

Figure S59. Analytical SEC traces of (A) **T-H/PDI**, (B) the crude reaction mixture, and (C) purified **C-T-PDI**.